UiT The Arctic University of Norway

Faculty of Health Sciences, Department of Pharmacy

Drug Transport and Delivery Research Group

Zwitterionic antimicrobial nanoparticles for biofilm therapy

Anna Ngoc Phung

Master's thesis in Pharmacy, May 2021

Supervisors: Dr. Sybil Obuobi and Professor Nataša Škalko-Basnet

ACKNOWLEDGEMENT

This project was carried out at the Drug Transport and Delivery Group, Department of Pharmacy at the University of Tromsø (UiT) – The Arctic University of Norway from September 2020 to May 2021.

First and foremost, I want to express my deepest gratitude to my main supervisor, Dr. Sybil Obuobi, for the opportunity to work on this project and write my master thesis with you. I am so honored and grateful that I got to collaborate with you. Thank you for the patience, the exceptional guidance and for sharing your endless knowledge with me. I am sincerely grateful for your continuous encouragement and support, which have made this project so enjoyable and given me the motivation and courage to strive for the best.

Secondly, I would like to express my great appreciation towards my co-supervisor, Professor Nataša Škalko-Basnet, for introducing the field of nanomedicine to me, which sparked my interest for the topic. Heartful thanks for the continuous advices and caring support, I am very privileged to get the opportunity to study under your guidance.

Special thanks to all professors and PhD students working at the Drug Transport and Delivery Group for providing such a positive and pleasant project environment. Especially thanks to our principal engineer, Martin Skipperud Skarpeid, for all the technical help at the laboratory.

I would also direct my appreciation to the Research group for Host Microbe Interactions (HMI) at Department of Medical Biology, in particular senior engineer Kjersti Julin, for your precious time providing me with materials and allowing me to work at the laboratories. I also want to thank Tom-Ivar Eilertsen, Randi Olsen and Augusta Hlin Aspar Sundbø at Advanced Microscopy Core Facility (AMCF) for your valuable guidance and contribution when using microscope instrumentations. I am very grateful for all your help.

Finally, my deepest and sincere gratitude goes to my family, friends, boyfriend and fellow pharmacy master students. Thank you all so much, for the love, endless support and for always believing in me.

ABSTRACT

In recent years, many pathogenic bacteria have developed resistance against the existing antimicrobials, a phenomenon known as antimicrobial resistance (AMR). One of the many reasons contributing to the observed failure of current therapies, is the poor drug penetration across the microbial biofilm. Biofilms are small structural communities of bacterial cells that excrete an extracellular polymeric substance. They are involved in the pathogenesis of many diseases and account for up to 80% of all human bacterial infections. Nanotechnology based drug delivery systems (DDS) can enhance the therapeutic efficacy of conventional antimicrobial drugs but very few possess responsiveness to the biofilm milieu. This project therefore seeks to develop a zwitterionic nanoparticle, which leverages on the biofilm microenvironment (i.e. acidic milieu, bacterial enzymes) to control the behavior of the DDS against *Staphylococcus aureus* biofilms.

DNA nanogel loaded with vancomycin was fabricated by a two-step annealing method and incorporated into zwitterionic liposomes via the thin-film hydration method to prepare a series of zwitterionic nanoparticles. Characterization of the most optimal formulation was done by dynamic light scattering (DLS). *In vitro* drug release profile was evaluated in the absence/presence of lipase. Biofilm binding, penetration, inhibition and eradication using the formulations was evaluated via crystal violet staining, scanning electron microscopy (SEM) and confocal microscopy (CLSM). The toxicity and translational value of the formulation was evaluated against HaCaT cells and in an *ex vivo* porcine skin explant model respectively.

The most optimal zwitterionic nanoparticle formulation, PDM 90/5/5, had an average size of 220.63 ± 0.84 nm, exhibiting a zeta potential of +0.02 ± 0.02 mV at physiologic pH and +15.23 ± 0.21 mV at acidic pH. Cumulative release of the PDM 90/5/5 formulation in presence of lipase 8 mg/mL was 88.76 ± 14.95% after 24 h compared to the release profile in the absence of lipase (49.57 ± 1.46%). PDM 90/5/5 effectively inhibited and eradicated *S. aureus* biofilms *in vitro* and *ex vivo*. Toxicity studies on HaCaT cells revealed negligible toxicity.

In conclusion, zwitterionic nanoparticles able to enhance the delivery of vancomycin against *S. aureus* wound biofilms were successfully developed. The formulation demonstrated pH and enzyme responsiveness, enhanced biofilm binding and controlled the drug release.

Key words: pH-responsive drug delivery systems; nanoparticles; DNA nanotechnology; liposomes; biofilm; wound infection

ABSTRACT (NORWEGIAN)

I de siste årene har mange patogene bakterier utviklet resistens mot eksisterende antimikrobielle legemidler, et fenomen kjent som antimikrobiell resistens (AMR). En av de mange grunnene som bidrar til dagens observerte terapisvikt, er den dårlige penetreringen av legemiddel gjennom biofilm. Biofilm er små strukturelle samfunn av bakterielle celler som skiller ut en ekstracellulær polymerisk substans. De er involvert i patogenesen av mange sykdommer og er ansvarlig for opp til 80% av all infeksjon. Nanoteknologibaserte drug delivery systems kan forbedre den terapeutiske effekten av konvensjonelle antimikrobielle legemidler, men svært få systemer innehar sensitivitet til miljøet i biofilm. Dette prosjektet ønsker dermed å utvikle en zwitterionisk nanopartikkel, som utnytter biofilmens mikromiljø (lav pH, bakterie-enzymer) for å kontrollere oppførselen av drug delivery systemet mot *Staphylococcus aureus* biofilm.

DNA nanogel med vancomycin ble fabrikert via en to-trinns hybridiseringsmetode og inkorporert i zwitterioniske liposomer via «thin-film hydration method» for å preparere en serie av zwitterioniske nanopartikler. Karakterisering av den mest optimale formuleringen ble utført via dynamisk lysspredning (DLS). *In vitro* legemiddelfrigjøringsprofil ble evaluert med eller uten tilstedeværelse av lipase. Biofilm binding, penetrering, inhibering og utrydning ved bruk av formuleringene ble evaluert via farging med krystallfiolett, sveipelektronmikroskop (SEM) og konfokal mikroskop (CLSM). Toksisitet og den translasjonelle verdien av formuleringen var evaluert henholdsvis mot HaCaT celler og i en *ex vivo* grise-huds explant modell.

Den mest optimale zwitterioniske nanopartikkel-formuleringen, PDM 90/5/5, hadde en gjennomsnittlig størrelse på 220.63 ± 0.84 nm, med et zeta potensial på +0.02 ± 0.02 mV ved fysiologisk pH og +15.23 ± 0.21 mV ved lav pH. Den kumulative frigjøringen fra PDM 90/5/5 formuleringen med tilstedeværelse av 8 mg/mL lipase var 88.76 ± 14.95% sammenlignet med frigjøringsprofilen ved fraværelse av lipase (49.57 ± 1.46%). PDM 90/5/5 inhiberte og utryddet *S. aureus* biofilm effektivt både *in vitro* og *ex vivo*. Toksisitetsstudier på HaCaT celler viste ubetydelig toksisitet.

Til konklusjon ble suksessfulle zwitterioniske nanopartikler utviklet for forbedret transport av vancomycin mot *S. aureus* biofilm i sår. Formuleringen demonstrerte en pH- og enzymresponsiv effekt, forbedret biofilm binding og kontrollerte legemiddelfrigjøringen.

Nøkkelord: pH-responsiv drug delivery system; nanopartikler; DNA nanoteknologi; liposomer; biofilm; sårinfeksjon

TABLE OF CONTENTS

LIST OF TABLES

LIST OF FIGURES

ABBREVIATIONS

AMR	Antimicrobial resistance
CHEMS	Cholesteryl hemisuccinate
CV	Crystal violet
CLSM	Confocal laser scanning microscopy
DAP	Diaminopimelic acid
DDS	Drug delivery system
DLS	Dynamic light scattering
DMEM	Dulbecco's Modified Eagle's Medium
DMSO	Dimethyl sulfoxide
DN	DNA nanogel
DNA	Deoxyribonucleic acid
DODMA	1.2-Dioleyloxy-3-dimethylaminopropane
EE	Entrapment efficiency
EB	Elution buffer
ECM	Extracellular matrix
EPS	Extracellular polymeric substance
EPR	Enhanced permeability and retention
FBS	Fetal bovine serum
GFP	Green fluorescent protein
H_2O_2	Hydrogen peroxide
kDa	Kilodalton
LPS	Lipopolysaccharide
MIC	Minimum inhibitory concentration
MMP	Matrix metalloproteinase
MTT	3-(4.5-dimethylthiazol-2-yl)-2.5-diphenyltetrazoliumbromide
NAG	N-acetylglucosamine
NAM	N-acetylmuramic acid
OD	Optical density
PBS	Phosphate-buffered saline
PDI	Polydispersity index
PEG	Polyethylene glycol
RES	Reticuloendothelial system
ROS	Reactive oxygen species
SD	Standard deviation
SPC	Soy phosphatidylcholine
SEM	Scanning electron microscopy
TEM	Transmission electron microscopy
TSB	Tryptic soy broth
QS	Quorum sensing

1 INTRODUCTION

1.1 Antimicrobial resistance

Since Alexander Fleming discovered penicillin in 1928 and the mass production of the antibiotic began in the 1940's, millions of lives have been saved from the deadly effects of infectious diseases (1, 2). In recent years however, many pathogenic bacteria have adapted to develop resistance against many of our antimicrobial arsenal; a phenomenon commonly known as antimicrobial resistance (AMR). Although resistant bacterial strains arise throughout nature via a process known as natural selection, the overuse and misuse of antibiotics in agriculture or livestock and the arbitrary prescription of antimicrobials are major factors that have escalated AMR (3). Yet, only in the last decade has global interest in AMR increased worldwide. This increasing public health concern on AMR can be attributed to the significant number of clinical isolates bearing drug-resistant genes to last line antibiotics (4). Consequently, the World health organization (WHO) has declared AMR as a major global threat to public health for which new therapies are warranted.

Currently, recurrent infections due to AMR are common as a large number of conventional antibiotics are no longer successful in the clinical management of bacterial infections. AMR is defined as the ability of microorganisms to withstand exposure to antimicrobial agents. It is well known that all organism have to fight for their own survival and bacteria is no exception. To protect themselves against tough environments and from host defense mechanisms, bacterial pathogens are required to develop strategies to survive. Among the many reported strategies, mechanism that expel and negate drug agents (i.e. through influx/efflux alteration of drug agent), modify the bacterial target site or form biofilms are known to lead to the emergence of AMR (5). These mechanisms can be driven by alterations in the genetic material of bacteria, such as a random endogenous point mutation which can up- or down- regulate genes to alter protein expression and behavior in bacteria (3, 6). Subsequently, through horizontal gene transfer, mobilization of the resistance gene among the entire bacteria population is initiated. The mutant bacteria can also transmit the resistance features to other bacteria via plasmid exchange and the receiving bacteria can then obtain that foreign deoxyribonucleic acid (DNA) (3). Through these strategies bacteria pathogens can oppose antimicrobial agents, making the conventional antimicrobials less effective or inadequate as treatment of bacterial infections. The introductory section of this thesis seeks to provide basic biological information about bacterial pathogens and the formation of biofilms as a major factor that contributes to their

resistance and tolerance against antimicrobials. Further on, the challenges attributed to antimicrobial therapy of biofilms will be discussed, and lastly a promising field of smart drug delivery strategies to combat the escalated AMR will be presented.

1.2 Bacterial pathogens

Bacteria are a type of prokaryotic cells with typically a length and diameter of only a few micrometers. They exist in different sizes and shapes; for instance, spherical shape like *Streptococcus*, rodlike-shaped like *Escherichia coli* or spiral-shape like the *Treponema pallidum* (7). The differences in the bacteria size, shape, living-standards and survival mechanisms make the myriad of bacteria very diverse in behavior. Unlike eukaryotic cells, bacteria lacks a membrane-bound nucleus in addition to organelles in the cell membrane, e.g. mitochondria. The genetic material of bacteria lies in the cytoplasm and consists typically of a single molecule of double-stranded DNA, often having an irregular shape. Bacteria may also possess *plasmids*, which are extrachromosomal genetic materials in a circular closed ring (8).

Bacteria can be categorized into two groups; Gram-positive and Gram-negative bacteria. The difference is mainly found in their cell wall, a structure that gives the bacteria it's integrity. While the Gram-positive bacteria has its peptidoglycan composed of long sugars and amino acid polymers as the primarily component, the Gram-negative bacteria has a more complex composition. The cell wall in Gram-negative bacteria is composed of the same peptidoglycan as in Gram-positive bacteria but is of a thinner layer and has an additional outer membrane containing lipids, other proteins and lipopolysaccharides which gives it a rigid structure (9, 10). The synthesis of the peptidoglycan is complex. Its polymeric backbone consists of alternating aminosugars; *N*-acetylglucosamine (NAG) and *N*-acetylmuramic acid (NAM), wherein the latter is attached to a tetrapeptide side-chain consisting of L-alanin, D-alanin, D-glutamic acid and either L-lysine or diaminopimelic acid (DAP). The tetrapeptide is responsible for the cross-linkage to glycine residues, and these glycine residues will further attach to a new section of a tetrapeptide forming the structural peptidoglycan lattice (8, 10).

For bacteria pathogens commonly susceptible to antimicrobials, they usually cause systemic infections in their free-living, planktonic form, which is often easily treatable. However, bacteria can also colonize solid or non-solid surfaces by attaching to each other to form sessile state biofilms (11). These complex communities of cells are much more resilient to antibiotics,

consequently making biofilm one of the main mechanism contributing to the reduced therapeutic efficacy of antimicrobials (12).

1.3 Biofilm infections

Biofilm formation is involved in the pathogenesis of many diseases and is responsible for up to 80% of all human bacterial infections (13). Because the biofilm infections are highly resistant to antimicrobials, they are highly persistent and are major causes of treatment failure in clinics. Pathogens frequently associated with biofilms include *Pseudomonas aeruginosa*, *Staphylococcus aureus* and *Escherichia coli* (14). Biofilms are described as small structural dynamic communities of bacterial cells that excrete an extracellular polymeric substance also called the exopolysaccharide (EPS). The EPS in addition to proteins, enzymes and extracellular DNA forms a crucial self-generated and very much protective heterogenous environment called the extracellular matrix (ECM) (15, 16). While the components of the matrix varies among bacteria, the ability to irreversibly adhere to and colonize different surfaces and tissues is common (17).

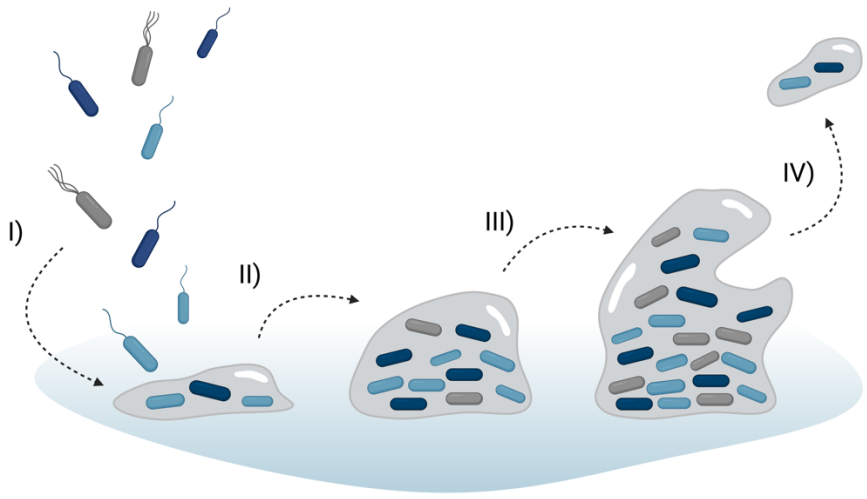

Figure 1: *Biofilm formation stages.*

There exist multiple pathways responsible for the formation of biofilm. Biofilm formation is triggered by several environmental cues, occurs via several steps, and is collectively coordinated in a bacteria population through quorum sensing (QS) signaling between bacteria

cells (18). QS is a cell-cell chemical communication strategy of the bacterial community which relies on small signaling molecules, called autoinducers, to integrate and deliver information to coordinate the pathogenic activity (19). Through the accumulation and detection of these autoinducers in the extracellular environment, the regulation of gene expression can take place collectively to regulate biofilm formation and maturation (20). The different formation stages of biofilms (**Figure 1**) can be divided into four phases namely; I) the initial adsorption and contact attachment of bacteria to the surface, II) formation of the micro-colony and release of EPS, III) development of architecture and maturation of biofilm and the IV) detachment of cells and start of new cycle on a new surface (21). Biofilm formation is, as abovementioned, controlled by multiple pathways as well as diverse genes, which can alter the metabolic activity compared to their planktonic state. For instance, specific genes and intracellular molecules regulate the expression of adhesion ligands during the formation of biofilms. Additionally, in *P. aeruginosa* biofilms, studies have shown that genes involved in EPS synthesis are upregulated (22). Concordantly, genes encoding enzymes involved in glycolysis and fermentation have also been found to be upregulated in *S. aureus* (23). This alteration in gene expression will further alter the microenvironment to better protect and develop the biofilm community. These diverse genetic alterations make the biofilms highly adaptable and persistent.

Compared to the healthy tissues and to the planktonic bacterial environments, the biofilm microenvironment is characterized by various unique features such as low pH, high levels of hydrogen peroxide (H_2O_2) and low oxygen due to the EPS and the fermentation of bacteria within the biofilm (24). The fermentation process results in acidic byproducts that in the presence of high glucose will accumulate and decrease the pH value in the biofilm. Components of the matrix, i.e. cytoplasmic proteins, also generates an acidic habitat for the bacteria cells during biofilm formation, typically pH as low as 4.5, which can further induce excretion of the EPS and the persistent accumulation and longevity of the biofilm (16, 25, 26). In the biofilm microenvironment, high levels of H_2O_2 have also been shown to promote biofilm formation through promotion of alginate production in mucoid *P. aeruginosa* (27) or induction of the EPS production in *Acinetobacter oleivorans* (28). The high levels of reactive oxygen species (ROS) or H_2O_2 can increase oxidative stress, which induces cell and tissue damage (29, 30). On the other hand, low levels of oxygen and nutrition scarcity are other key-characteristics of the biofilm microenvironment occurring partly due to bacterial consumption. This oxygen restriction forms anaerobic sites within the biofilm, reducing metabolic activity and

consequently impeding bacterial cell growth (31). As a result of this altered chemical environment, the development of persistent biofilm and the bacterial stationary phase of growth contribute to the ineffectiveness of antimicrobials. While the abovementioned unique characteristics of biofilm infections allow manipulation of carrier systems, the acidic environment remains one of the most widely explored targets for the design of nanocarriers.

Biofilm colonization can cause infections in both acute and chronic skin wounds (32), on medical exogenous devices and on prosthetics, as well as play a key role in many bacterial diseases such as cystic fibrosis or endocarditis (11, 17). Skin wounds are damaged tissue, which although contains both endogenous and exogenous microorganisms, normally heals successfully. However, some acute and chronic wounds, such as pressure ulcers, are delayed and prevented from healing in a timely manner due to biofilm infection (11). The chronic wound environment is highly susceptible to biofilm formation due to the presence of highly necrotic tissues and impaired immune responses that encourage bacteria attachment and colonization (**Figure 2**) (33).

Several physiological pathways are responsible and involved in wound healing and reconstruction of skin tissue. Normally, there is a balance between growth factors, enzymes and other tissue repairing proteins which are responsible for successful wound healing and formation of scar-tissue. However, when a matured biofilm community is present in the wound, the bacterial infection disturbs this balance indirectly through alteration in the expression of these repairing molecules and directly through the formation and introduction of destructive enzymes and toxins (11). For instance, the activity of a group of enzymes called matrix metalloproteinases (MMPs), which are responsible for the normal growth and tissue turnover through degradation of proteins in the extracellular matrix, are found to be upregulated by bacteria derived enzymes (34). MMPs plays a crucial role in the reformation of skin tissue, and recently also found to co-regulate different molecules in inflammation and immunity responses. Increased MMP activity can lead to irregular cell proliferation and undesired tissue damage. Furthermore, proteases released from bacteria (e.g. *P. aeruginosa*), influence the degradation of proteins from fibroblasts to impair cell growth in tissues. These enzymes are also found to impair immune responses from the host cell (35).

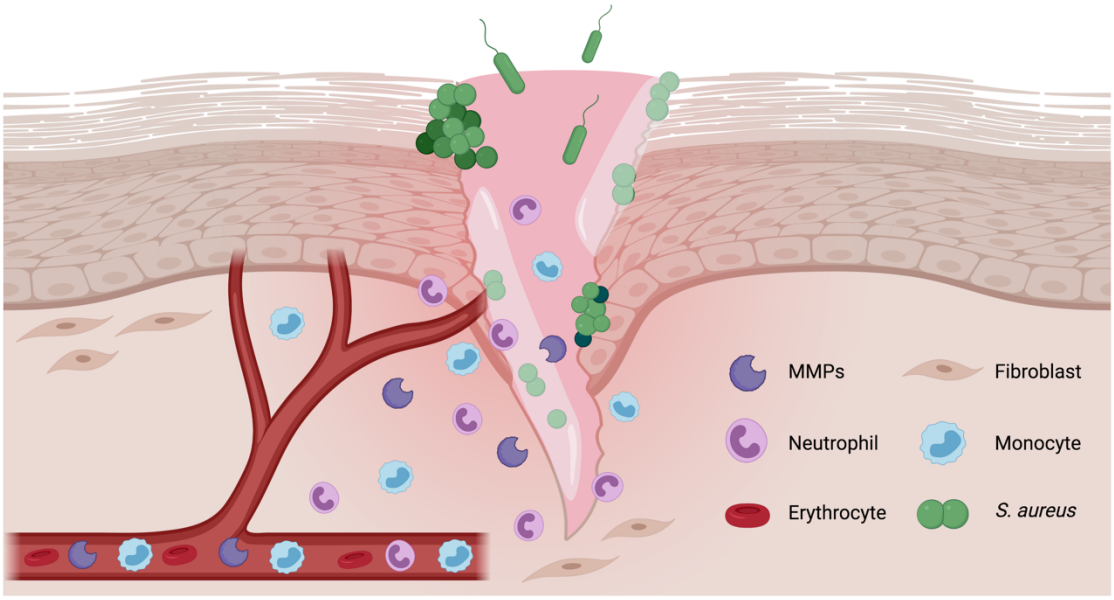

Figure 2: *Illustration of a cutaneous wound bed and the migration of cells.*

During infections, changes in gene expression and an excessive increase of intracellular signaling molecules contribute to the activation of immune response at the infection site. Unlike planktonic cells which are easily cleared by the polymorphonuclear neutrophils and macrophages, the deeply embedded bacterial cells within the biofilm are much more resistant which reduces the effectiveness of immune cell clearance (36). In fact, the infiltration of these cells further enhance biofilm formation and also contribute to the chronic inflammatory state of the biofilm environment. The enhanced inflammation state of the wound biofilm further contributes to the altered pathophysiology (11). Additionally, infiltration and penetration of antimicrobials to the embedded pathogenic bacteria residing in the deep layers of biofilm is more challenging. Panels of studies have explored the use of conventional antibiotics to improve clearance of biofilm infections, however several authors have reported biofilm resistance and tolerance to antibiotics, through mechanisms that are attributed to phenotypic heterogeneity instead of the "traditional" inherited genetic antibiotic resistance (37-39). Consequently, conventional antimicrobial therapy against biofilms treatment faces many obstacles. The next section describes the challenges attributed to antimicrobial therapy and current strategies to address biofilm infections.

1.4 Challenges of antimicrobial therapy against biofilms

In addition to the presence of resistance genes, limited and incomplete antimicrobial diffusion due to the EPS matrix, oxygen and nutrient deprivation within the chemically altered biofilm microenvironment, the development of persisters contribute to biofilm recalcitrance toward antimicrobial agents (21, 40). Several biofilm forming microbial species have been found to display this antibiotic tolerance. For instance, Ceri and colleagues assessed in 1999 the susceptibility of *E. coli*, *P. aeruginosa* and *S. aureus* to different antibiotics (e.g. ampicillin, ciprofloxacin, tobramycin, vancomycin). They reported that the minimal inhibitory concentration (MIC) of the bacterial biofilms was 100 to 1000 times higher as compared to the planktonic cells. Thus indicating that the antibiotics were less effective against biofilm embedded bacteria, and that the biofilm presented tolerance like features against the drugs (41).

Antimicrobial drug permeability through the biofilm is affected by the EPS components (i.e. polysaccharides, proteins, DNA and other waste molecules) which can interact with the antimicrobial to delay its penetration throughout the biofilm matrix. Moreover, the antibiotic may also be antagonized or enzymatically degraded before reaching its target site (21, 42). Another crucial aspect is the difference in physiological activity throughout the biofilm, where the metabolic activity in the biofilm core is lesser compared to the outer parts. This is due to the scarcity of oxygen and nutrition, developing anaerobic sites within the biofilm (43). Aminoglycosides are an example of an antibiotic subclass that have been reported to be less active at anaerobic conditions compared to aerobic conditions, partly because they are dependent on oxygen for membrane transport. The rate of bacterial cell growth is subject to environmental changes (44). As a result of oxygen depletion, the bacteria within the biofilm enters a stationary, slow- or non-growing phase which consequently makes antibiotics targeting bacteria at the phase of exponential cell growth and multiplication (i.e. synthesis of cell wall or DNA replication) much more ineffective (45). For instance, penicillin which targets synthesis of the growing peptidoglycan cell wall (46) , will not be as effective if it was to act on cells in the stationary phase. Eng and coworkers studied back in 1991 the bactericidal effect of several antibiotics on different bacteria in their growing and non-growing phase. They concluded that the antibiotic killing activity of the different test agents were dependent on the growth phase of the bacteria cells, reporting for instance that no antibiotics were bactericidal against non-growing strains of *S. aureus* (47).

A small percentage of this population of non-growing bacteria cells can also differentiate to persisters, a subpopulation of *S. aureus* first introduced by Bigger in 1944. The subpopulation survived a bactericidal concentration of penicillin, showing much higher resistance compared to its other genetically homogenous bacteria cells (48). Since then, numerous of other different microbial species have been found to obtain these persisters, playing a crucial part in the phenotypic antibiotic tolerance of biofilms (49-51). This phenotypic heterogeneity or variation is a natural and present feature of bacteria cells due to the cell to cell variation in the population, showing that antimicrobial tolerance is not only obtained through alterations in the genome but could also be attributed to the dormant-like state of differentiated bacteria (52, 53).

Nevertheless, biofilm related infections, like many other bacterial infections, are commonly treated with conventional antibiotics. Current strategies to address the biofilm-associated antimicrobial tolerance include high concentrations of topical antibiotics with the advantage of minimizing systemic side effects (53). Another emerging strategy is the combined use of antimicrobials with adjuvants to improve the drug therapeutic efficacy, an area where nanotherapeutics have gained significant recognition over the last decade as novel and smart drug delivery systems (DDS) (54). The following table present a summary of current antibiotic treatment regimen for biofilm infections in Norway (**Table 1**).

Table 1: *Summary of current antibiotic treatment regimens according to biofilm infection site in Norwegian hospitals (55).*

Biofilm infection site	**Antibiotic regimen***	**Duration***
Endocarditis	2 g cloxacillin (6 times daily) (IV).	42 days
Intravascular catheters	2 g cloxacillin (4 times daily) + 5 - 7 mg/kg gentamicin (daily) (IV).	5 days – 6 weeks depending on agent Gentamicin should only be used for some days
Odontogenic infections (complicated)	1.2 g benzylpenicillin (4 times daily) + 1 g metronidazole (daily) (IV), followed by 1 g phenoxymethylpenicillin (4 times daily) + 400 mg metronidazole (3 times daily) (oral).	7 days

Orthopedic prosthetic infections	2 g cloxacillin (4 times daily) (IV), followed by 300 – 450 mg rifamphicin (2 times daily) (oral) + 750 mg ciprofloxacin (2 times daily) (oral).	1 – 2 weeks 3 months (after cloxacillin) 3 months (after cloxacillin)
Postoperative, deep cutaneous wounds	1 – 2 g cloxacillin (4 times daily) (IV). 2 g cefotaxime (3 times daily) (IV).	7 – 10 days 7 – 10 days
Rhinosinusitis	1.2 g benzylpenicillin (4 times daily) (IV).	7 days

** The antibiotic regimen and duration period depend on i.e. type of bacteria, severity of infection, allergies*

1.5 Nanomedicine: A tool to combat AMR

Despite the growing challenge of AMR and the necessity to develop new antibiotics, the clinical antimicrobial pipeline has been stagnant for years. Slow development of pre-clinical candidates, poor clinical translation and absence of economic interest and incentive are some of the reasons contributing to the weakened pipeline (56). To address the poor bioavailability (i.e. unsatisfactory drug penetration, accumulation and poor specificity) of our current antimicrobial drugs, the use of innovative delivery systems that can improve the therapeutic efficacy of antimicrobial against resistant pathogens are urgently needed (57).

Over the last decade, nanomedicine has gained a lot of interest as a field of science and technology that relies on the use of nanosized carrier systems to diagnose, treat and prevent diseases. The nanosized materials are normally classified as nanoparticles or nanocarriers of sizes smaller than 100 nm; although flexibility in size has been shown in practice (57). Nanocarriers are nanomaterial colloidal systems, that act as transport vehicles for drug ligands. Typical examples of different nanocarriers include, but not limited to, liposomes, micelles, polymeric nanoparticles and dendrimers. These nanocarriers have demonstrated significant improvement in physiochemical properties, drug release pharmacokinetic properties and also reduced the toxicities. Additionally, the utilization of nanotechnology based drug systems have resulted in improved design of delivery systems and successfully enhanced the therapeutic efficacy of conventional drugs (6, 57).

Nanotechnology has for instance been applied in cancer therapy for several years, and a variety of formulations are in clinical trials or available on the market. Doxil® for instance, containing

doxorubicin for treatment of metastatic breast cancer, was the first nanoparticle based drug formulation that was approved and now available on the market (58, 59). It is demonstrated that angiogenesis in tumor sites leads to a higher vascular density and enlarged endothelial cell gap, making the tissues more prone to extravasation and retention of molecules. Due to this enhanced permeability and retention (EPR) effect in tumor tissue, the drug ligand can accumulate at the tumor site via passive targeting. This effect is also seen at infection sites with inflammation and lowered pH values (60); forming the basis of exploring the application of nanocarriers in infectious diseases.

In recent years, nanotechnology-based stimuli-responsive drug delivery systems (DDS) have gained interest as novel tools to deliver antimicrobials against resistant pathogens in response to environmental or biological stimuli and have been designed to potentially possess antimicrobial activity themselves (61). These nanosystems offer many advantages as a drug delivery system for antimicrobials, such as optimization of the physiochemical properties of the antibacterial drug, provide protection, increase stability, effectively transport drug ligand near target site and offer enhanced bacterial membrane interaction (6, 62). A combination of conventional antimicrobials with stimuli-responsive materials or other agents that utilize a different mechanism of action not attributed to the essential survival pathway of the bacteria pathogen, can lower the potential risk of AMR. The DDS can e.g. act by enhancing the bacteria cell permeability or diminish and disrupt the biofilm (15).

Authors have demonstrated that these nanosystems have the ability to aid the penetration of antimicrobials into the matrix, disrupt biofilms and bring drugs closer to interact with the deeply embedded bacteria pathogens (61, 63, 64). The subsequent sections will focus on the use of these nanocarriers in drug delivery by focusing on liposomal and DNA based systems.

1.6 Liposome as a nanocarrier system

Liposome based drug delivery systems have been successfully explored as nanocarriers in the treatment of cancers, fungi and bacterial infections (65). Liposomes are described as spherical phospholipid vesicles normally composed of an aqueous core which is surrounded by one or several lipid bilayers (66). Commonly used natural phospholipids for preparing liposomes include phosphatidylcholine or soybean lecithin. The amphipathic nature of these vesicles can generate a bilayer (unilamellar), several bilayers (multilamellar) or micelles with a hydrophobic

core. The classification of the liposomes is often based on their surface characteristics (i.e. conventional, cationic, PEGylated or ligand-targeted liposomes) (**Figure 3**) but can also be determined based on the number of bilayers (lamellarity), size measurements or by the type of preparation method used (67). There are two techniques for developing drug-loaded liposomal preparations; passive loading and active loading. In passive loading, the drug is encapsulated in the liposomes during the development process, whereas in the active loading technique, the drug is incorporated after preparing the liposomes. The passive loading technique include methods such as the mechanical dispersion method, solvent dispersion method or detergent removal method. The lipid film hydration method, which is a subtype of mechanical dispersion method, is the most commonly used technique to prepare liposomes. All the aforementioned methods can be defined by 3 basic steps; the drying of the lipids from an organic solvent, re-dispersion of the lipids in an aqueous media and the size reduction step to obtain the targeted size (65, 68).

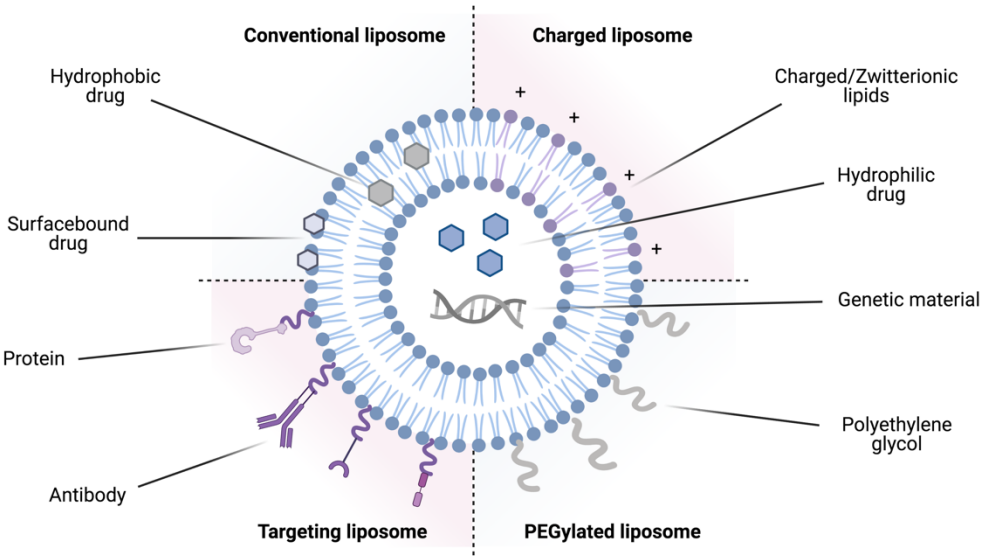

Figure 3: *Different surface modification strategies of liposomes.*

There are several advantages of liposomes as a drug carrier vehicle. For instance, they are biocompatible, very well tolerated, enable the entrapment of hydrophilic, hydrophobic or amphiphilic drug ligands and offer a myriad of formulation optimization options. Additionally, liposomes resemble the cell membrane and can mimic the biological cell structure due to the lipid bilayer (66, 69). The use of liposomes as delivery systems has improved drug targeting,

therapeutic potential and stability of the cargo as well as reduced toxicity (70). In antibacterial therapy, their use has been viewed as a measure to address drug resistance, systemic inactivation of antibiotics and potential toxicities after administration (71). These nanocarriers have demonstrated efficient and controllable intracellular delivery of antimicrobials due to their ability to fuse with bacterial membranes to increase the activity of the antibacterial as compared to the free drug (72-74).

The surface properties of liposomes are determined by the hydrophilic head of the phospholipids. The surface charge of liposomes is typically in a neutral range which corresponds to an estimated zeta potential ranging between -10 mV to + 10 mV (75, 76). Zeta potential, which is a surface charge characterization technique, can for instance be utilized (to some extent) to predict the degree of stability of the liposome suspension (or other nanosuspensions of other materials). In order to be stable and have sufficient repulsive force, the zeta potential of the liposomal suspension is required to be lower than -30 mV or higher than +30 mV. At these values, the liposomes are less prone to increase in size and form agglomerates (77). Anionic liposomes (negative zeta potential) are more easily cleared by the reticuloendothelial system (RES), whereas cationic liposomes (positive zeta potential) have a longer circulation half-life due to absorption of proteins in the blood, which will improve the stability of the nanocarrier. On the other hand, cationic liposomes have been reported to possess higher toxicity (e.g. in lung cells) as compared to neutral or anionic liposomes (78, 79). A desired zeta potential or surface charge of the liposomes can be obtained by modifying the liposome composition through addition of natural or synthetic lipids with specific electrical functions, and thus enhance the performance of the nanocarrier.

Modification of the surface through charge or addition of targeting moieties (such as antibodies or peptides) can further promote specific binding to target molecules (80, 81). For instance, a cationic formulation will better bind and interact with the anionic bacteria cell wall through electrostatic interactions. This will promote specific binding and enhance the therapeutic efficacy of the formulation. Another technique to optimize these nanocarriers includes the popular PEGylation design method, where the hydrophilic polyethylene glycol (PEG) polymer covalently attaches to the bilayer surface. This modification has been shown to enhance the circulation time and reduce immunogenicity because these “stealth” liposomes hide better from the RES via the inhibition of opsonization to present superior protection of the formulation (82). Moreover, the modification of the lipid composition can impart stimuli-responsiveness as a strategy to enhance and control the pharmacokinetic release profile of the drug. In such smart

systems, the nanocarriers can be designed to be reversible (i.e. zwitterionic liposomes) to specifically respond to environmental changes such as pH. Besides, the drug release can also be designed to be controlled by a stimulus, i.e. bacterial enzymes or toxins at infection sites (83).

Although nanocarriers such as liposomes have contributed to improve the physiochemical properties and pharmacokinetic profiles of drug molecules, limitations still exist. Poor drug loading efficiency and rapid elimination from the circulation system are some challenges these liposomal systems regularly encounter (70). Additionally, several formulation methods are expensive and reproducible batch preparation for larger-scale-use are often challenging (84). These limitations have given researchers an incentive to improve the stability and function of liposomes. Thus, to tackle some of the abovementioned limitations, hybrid systems composed of lipids and other materials have been developed (84). Incorporation of different polymers such as poly(lactic-co-glycolic acid) (PLGA) or polycaprolactone (PCL) has been reported to tackle obstacles like premature release of drugs and instability of liposomal formulations (85, 86). Furthermore, hybrid systems based on the combined use of liposomes and nucleic acid nanocarriers has also been explored as a promising field (62, 87). Thus, the next section will focus on the implementation of nucleic acids and their hybrids as smart materials and as antibacterial platforms.

1.7 DNA nanotechnology

Although a nascent field, DNA nanotechnology has been exploited as a tool for application in the biomedical fields such as bioimaging, sensing and diagnostics. This biomaterial has emerged as a novel and promising candidate for drug delivery systems (88). DNA structures can be an essential material and play a major role in the development of hybrid carrier systems, due to their enhanced biocompatibility, biodegradability, increased drug entrapment efficiency potential and improved cellular uptake compared to the pristine nanocarrier system (89, 90). DNA is a natural molecule in all living organisms which carries the complex genetic information and instructions to make proteins in our body (91). The DNA consist of double polynucleotide strands, which are the building blocks of the DNA backbone, consisting of 3 main components; a phosphate group, a pentose sugar and a nitrogenous base. The hydrogen bonds between the complementary bases relies on the Watson-Crick base pairing rule, where

adenosine binds to thymine, and guanine binds to cytosine. This base pairing model is the main principal when controllable DNA scaffolds are designed and fabricated to develop the DNA nanostructures (62, 91, 92). The cohesion of two "sticky ends" from complementary sequence motifs allows the bottom-up formation of complex but well defined two-dimensional (2D) and three-dimensional (3D) DNA assemblies with high predictability and versatility (93).

The invention of DNA nanotechnology started in the early 1980's when Nadrian Seeman studied the use of self-assembled DNA oligomers to develop DNA Holliday junctions for the crystallization of macromolecules (94). This strategy of DNA assembling and formation of complex DNA nanostructures has since advanced rapidly and evolved to two main techniques; the tile-based method and the DNA origami approach (62). The former technique, developed by Seeman and coworkers (95), is based on numerous repeated "tiles", small DNA bundles, which interconnect into well-defined lattices, due to hybridization of complementary single-stranded DNA extensions. The latter technique, invented by Paul Rothemund (96), utilizes a long single strand scaffold of DNA which is folded using numerous short staple strands to form arbitrary shaped structures to make the development of larger DNA arrays possible (97). By employing these approaches, various DNA nanocarriers have been developed, such as tetrahedrons (98), icosahedrons (99) and different origami structures (**Figure 4**) (100).

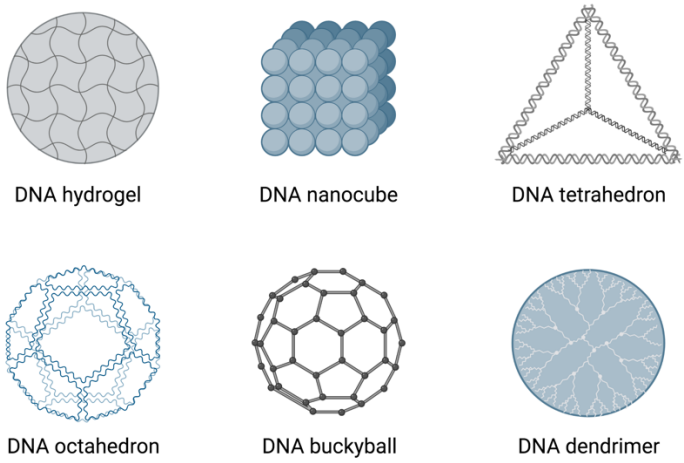

Figure 4: *Different types of DNA nanocarriers.*

In combination with other nanocarriers, DNA nanostructures have emerged as a promising hybrid system to further improve the efficacy of drugs. DNA nanostructures can be complexed

or conjugated with other moieties, either organic or inorganic materials such as hydrophobic liposomes or metal nanoparticles (e.g., gold or silver) respectively, to further enrich their functionality, improve their stability as well as specificity and make a multifunctional delivery system (62). The fusion of the hydrophilic backbone of DNA nanostructures with organic hydrophobic moieties (e.g. lipids) can increase the amphiphilic nature of DNA. This in return gives the DNA nanostructure the flexibility to deliver drugs, both hydrophobic and hydrophilic in nature (101).

The use of DNA nanotechnology and their hybrids has recently also been explored against resistant pathogens and their biofilms. Due to their greater ability to enhance the cellular uptake and accumulation, control the drug delivery and sustain the drug release, or to improve bacteria targeting specificity, these DNA scaffolds possess several advantageous strategies to enhance the therapeutic efficacy of drugs (62). For instance, Liu and coworkers studied in 2020 the effect of DNA tetrahedral nanostructure as a delivery vehicle for antimicrobial GL13K peptide against *E. coli* and *Porphyromonas gingivalis*. They reported that the DNA nanostructured delivery system enhanced antibacterial effect by increasing bacterial uptake, while also improving the stability of the peptide against *E. coli* (102). It has also been reported in another study by Zhang and colleagues that these nanostructures have the ability to modulate inflammation activity. These anti-inflammatory properties that this type of DNA nanostructure possesses can be utilized as an additional advantageous effect in the treatment of infections, e.g. skin wounds (103).

Although DNA nanostructures possess many advantages as smart drug delivery platforms, they still encounter some challenges in clinical translation. Studies on the nanocarrier's effect and performance done under lab conditions at cellular level (or even in animal studies, i.e. in mice) cannot always give a representative image and directly get translated to patients (62). Living organisms present complex physiology and biochemistry properties with biological microenvironments which can alter the designed DNA nanocarriers performance *in vivo*. A limitation of the DNA nanocarriers is their poor ability to reside within physiological environments. For instance, deoxyribonucleases (DNase) present in the serum can enzymatically degrade DNA, making the biological material unstable at physiological conditions. Another reason for degradation is the adsorption of serum-proteins, which can induce the opsonization effect leading to increased clearance by macrophages. Additionally, pristine DNA is also prone to fast clearance by the hepatic or renal system (93, 97). Besides the challenges of the stability of DNA nanocarriers and their performance *in vivo*, another aspect

that needs to be considered is the material expenses when synthesizing these DNA nanocarriers. To address the huge cost, optimization of manufacturing methods in a low-cost manner or development of amplification methods with high yields could be a solution (104-106).

There are numerous strategies available to tackle the obstacles DNA nanocarriers encounter. For instance, by crosslinking or chemically modifying the DNA backbone, the hydrolytic cleavage activity from DNases and subsequent degradation can be hindered and therefore enhance the nanocarrier's stability. Encapsulation, for instance by liposomes, is another possible strategy to enhance the stability of the DNA vehicle at physiological environments (**Figure 5**).

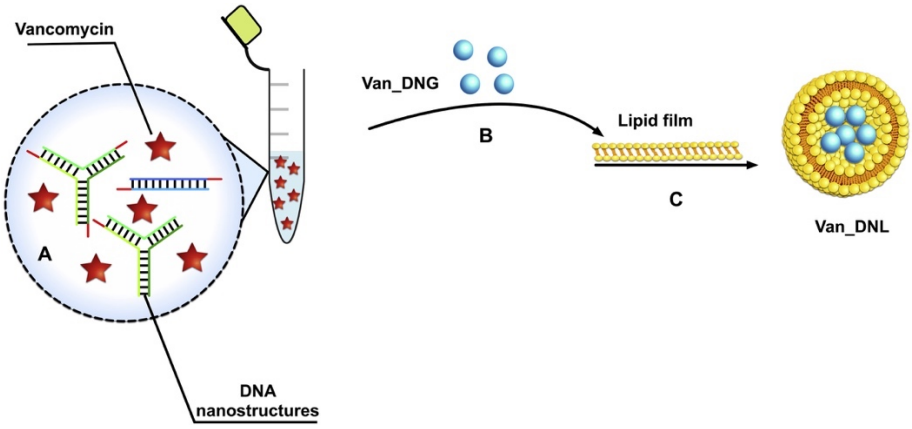

Figure 5: *DNA nanostructure encapsulation in a liposome. Reproduced with permission from (107).*

The DNA nanocarrier can be shielded by the lipid material, hiding the DNA from other macromolecules in serum and extracellular environment (97). Furthermore, enhancing the targeting properties by integrating stimulus responsive materials i.e. materials sensitive to microenvironments such as pH, temperature or specific enzymes, can improve the selective accumulation at target site as well as enhance the therapeutic efficacy of the drug delivery system.

1.8 Stimuli responsive nanocarriers against biofilm infections

The advancement of smart DDS with suitable functions are in urgent need to combat the limitations (i.e. low therapeutic efficacy as a result of poor specificity, low bioavailability, off-

target toxicity) of pristine DNA nanocarriers or their hybrid systems (83). A possible strategy to meet these current limitations is by introducing physical, chemical or biological stimuli responsive properties via the integration of smart moieties into the DDS. These modifications impart different chemical and structural properties that can be controlled by external triggers (i.e. light irradiation, magnetic, ultrasound) or by internal triggers (i.e. pH, temperature, enzymes) to enhance the pharmacokinetic release profile and improve the target specificity of the cargo. These tailored stimuli responsive DDS will minimize the adverse effects while enhancing the therapeutic efficacy of conventional drugs e.g. antimicrobials (108). A large number of literature exists that demonstrate cargo release triggered by external stimuli such as light irradiation (109, 110), electromagnetic radiation (111, 112) or ultrasound (113). These approaches are attractive options that have provided temporal precision among other advantages such as local release at target site, which will lower the systemic dosage needed and thus minimize side effects of the drug. Although these approaches are relatively non-invasive for the patients, some challenges such as low ease of use, limited penetration of the external force and possible damaging effect on surrounding healthy tissue still remains a problem and limits their application (108).

A different stimuli responsive approach is via the biological and internal triggered strategy by utilizing overexpressed enzymes or bacterial toxins present at the drug target environment. For instance, components of the biofilm matrix such as lipopolysaccharides or other present enzymes such as lipase are possible stimulus that could be harnessed (114). In 2011, Pornpattananangkul and colleagues presented an example of this strategy by utilizing a previously developed chitosan-modified gold nanoparticle stabilized liposome carrier (115) as a bacterial toxin-triggered drug release system for the treatment of bacterial infections. By binding cationic gold nanoparticles to the surface of the anionic liposomes, they could prevent liposome fusion as well as early cargo release. When the liposomes were present at bacterial infection site, the bacterial toxins could form pores releasing the modeled encapsulated antibiotic (vancomycin). They demonstrated that the formulation led to a methicillin-resistant *Staphylococcus aureus* (MRSA) inhibition as effective as an equal amount of vancomycin loaded non-stabilized liposomes and free vancomycin. Understandably, the novel approach showed enhanced stability and controlled the drug release to a much higher extent (116).

Using a similar concept, Chen and coworkers fabricated a pH and enzyme dual-responsive micelle drug delivery system for the release of antibiotics to treat alveolar injuries in lungs

caused by *P. aeruginosa*. Copolymers of poly(ethylene glycol)-poly(ε-caprolactone) (PECL) were conjugated with vancomycin to increase blood circulation time of the micelle and enhance specific targeting. Under acidic conditions, cleavage of the pH-cleavable hydrazine bonds between the copolymer and vancomycin would occur and result in the de-shielding and degradation of the micelles. Overexpression of present lipase enzymes degraded the enzyme sensitive poly(ε-caprolactone) moieties, and thus released the encapsulated ciprofloxacin. The results showed improved survival of infected mice, and bacterial burden was significantly reduced compared to the free drug and vancomycin-free micelles (81).

Over the years, strategies that leverage on the altered pH value at specific disease sites (i.e. tumor or bacterial infections) have also gained great interest in the scientific community. Many researchers have developed pH responsive nanocarrier systems for delivery of antimicrobials against biofilms. The biofilm microenvironment is characterized by changes in the pH value, giving rise to an increased acidic environment. This alteration in pH is therefore a very attractive target for researchers when developing novel drug delivery systems for biofilm infections (114). For instance, Lu and coworkers studied in 2018 the release of chlorhexidine and silver ions from the dual redox and pH sensitive mesoporous nanoparticles against oral biofilms. They concluded that in presence of low pH and glutathione, the cumulative release of chlorhexidine and silver increased (117). In 2020 Tian and colleagues also studied the ability of the pH responsive mixed shell polymeric micelles to enhance antimicrobial activity against *S. aureus* biofilms in mice compared to single shell polymeric micelles. They proposed that in the presence of acidic pH, the penetration and accumulation of mixed shell polymeric micelle nanocarriers with the drug model ciprofloxacin was significantly improved (118).

These studies show that modification of drug delivery systems to possess stimuli-responsiveness can enhance the therapeutic efficacy of antimicrobials and is an attractive field with a myriad of optimization possibilities. Owing to the growing knowledge of bacterial growth and the recalcitrance of biofilm, these stimuli responsive systems can be widely explored as an innovative approach to combat the growing AMR challenges as well as address obstacles of conventional antimicrobials. By leveraging on the inherent pH change, bacterial toxins or enzymes, the designed drug delivery system's pharmacokinetic release profile could be enhanced significantly.

2 AIM OF THE STUDY

The main objective of this study was to overcome the limitations of antimicrobial therapy (i.e. poor penetration, untimely degradation by bacterial enzymes) against *S. aureus* wound biofilms. Therefore, a zwitterionic liposome coated DNA nanogel system (herein referred to as zwitterionic nanoparticles) was designed to deliver antimicrobial drug. By leveraging the conditions of the biofilm microenvironments, this study sought to capitalize on the abundance of bacterial toxins (e.g. α-hemolysin), enzymes (e.g. lipase) and the inherent low pH condition in the biofilm environment to control the behavior of the nanocarrier. Advantageously, this would promote penetration of antimicrobials via improved biofilm binding, control drug release and effectively minimize the damaging effects of wound biofilm infections.

To achieve this, varying molar compositions of an ionizable cationic lipid (DODMA), ionizable anionic lipid (CHEMS) and a polysaccharide modified lipid (mannose) were incorporated into the lipid film to prepare an optimal zwitterionic system (**Figure 6**).

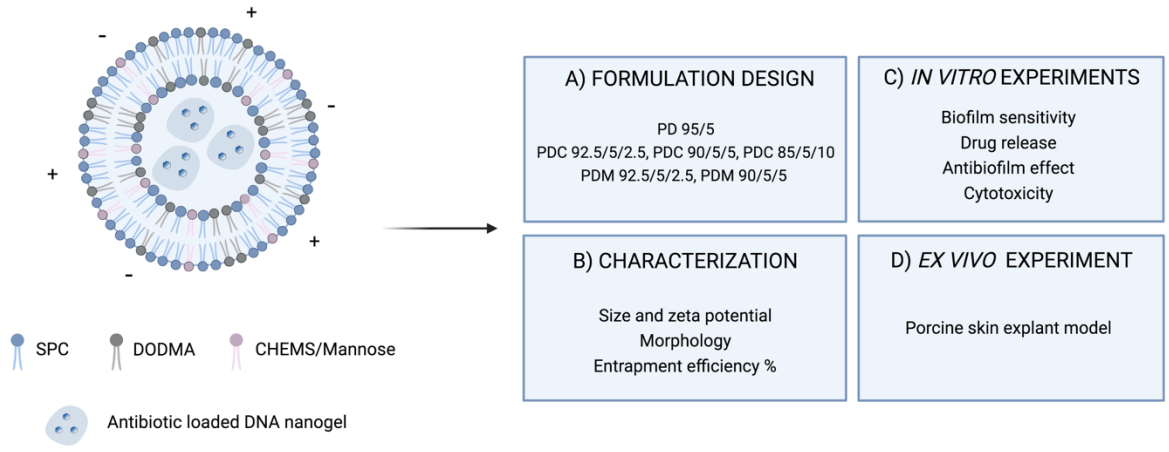

Figure 6: *Illustration of project plan.*

The characteristic properties of the different formulations, such as size, surface charge, drug release profile, toxicity, antibacterial and antibiofilm activity were investigated. Finally, an ex vivo porcine explant model was used to demonstrate the antibiofilm effect of the optimal formulation.

3 MATERIALS AND INSTRUMENTS

3.1 Materials

1.2-Dioleyloxy-3-dimethylaminopropane (DODMA), 16:0 PA-PEG3-mannose, cholesteryl hemisuccinate (CHEMS), 18:1 Liss Rhod PE were purchased from Avanti Polar Lipids (Alabama, USA). Lipoid S100 (soy phosphatidylcholine (SPC)) was a kind gift from Lipoid GmbH (Ludwigshafen, Germany). Uranyless was purchased from Electron Microscopy Sciences (USA). Methanol was purchased from VWR International S.A.S. (Fontenay-sous-Bois, France). 3-(4.5-dimethylthiazol-2-yl)-2.5-diphenyltetrazolium bromide (MTT), crystal violet 1%, Dulbecco Modified Eagle's medium (DMEM) high glucose, components of encapsulation buffer (EB) (5 mM Tris-HCL, 1 mM ethylenediaminetetraacetic acid (EDTA), 10 mM $MgCl_2$, 10 mM NaCl), α-hemolysin, lipase (from wheat germ, ~0.1 U/mL), Alexa Fluor 594 labelled lipopolysaccharide (LPS), phosphate-buffered saline (PBS) and vancomycin were purchased from Sigma Aldrich (Norway). Fetal bovine serum (FBS), human immortal keratinocytes (HaCaT), penicillin-streptomycin, *Staphylococcus aureus* NCTC 8325 pCM29 green fluorescent protein (GFP), tryptic soy broth (TSB) and trypsin were obtained from University hospital of North Norway (Tromsø, Norway). All the DNA sequences were purchased from Integrated DNA technologies (Belgium) and a detailed description of the sequences is provided (**Table 2**).

Table 2: *Oligonucleotide sequences for DNA nanogel preparation.*

CODE	DNA	OLIGONUCLEOTIDE SEQUENCE
Y-SAF	$Y\text{-}SAF_1$	GTCTTCGTCCTTATCGGTAGGGTGCTGAGCGGAATC CTGA
	$Y\text{-}SAF_2$	GTCTTCGTCCTTTCAGGATTCCGCTCAGTCATGTCATCAC
	$Y\text{-}SAF_3$	GTCTTCGTCCTTGTGATGACATGACACCCTACCGAT
Y-SAB	$Y\text{-}SAB_1$	ATCGGTAGGGTGCTGAGCGGAATCCTGA
	$Y\text{-}SAB_2$	TCAGGATTCCGCTCAGTCATGTCATCAC
	$Y\text{-}SAF_3$	GTCTTCGTCCTTGTGATGACATGACACCCTACCGAT
L-SAC	$L\text{-}SAC_1$	AAGGACGAAGACGTAGCCTACTATCTTCATTACCAGGTGCAGCC
	$L\text{-}SAC_2$	AAGGACGAAGACGGCTGCACCTGGTAATGAAGATAGTAGGCTAC

3.2 Equipment and devices

A detailed list of the various equipment and devices used in this project are provided below:

- BÜCHI Rotavapor R-124, Büchi labortecknik (Flawil, Switzerland).
- BÜCHI Vacuum Pump V-700, Büchi labortecknik (Flawil, Switzerland).
- BÜCHI Waterbath B-480, Büchi labortecknik (Flawil, Switzerland).
- Centrifugal filter units 50kDa, Sigma Aldrich (Norway).
- Cellophane membrane barrier, Zellglas (Germany).
- Dialysis membranes MW cut-off of 12-14kDa, Thermo Fischer Scientific (Norway).
- EM CPD300 Critical Point Dryer, Leica (Wetzlar, Germany).
- Multi-station Franz diffusion cell system, PermeGear Inc. (USA).
- Nucleopore® Track-Etch Polycarbonate Membranes 0.2 μm , 0.4 μm, 0.8 μm Whatman International Ltd. (UK).
- Polaron Range Sputter Coater, Quorom Technologies Ltd. (UK).
- Scanning electron microscope model Sigma and GeminiSEM 300, ZEISS (Germany).
- Sension+ PH31 pH-meter, Hach (Loveland, USA).
- Spark multimode microplate reader, Tecan (Switzerland).
- Transmission electron microscope model HT7800, Hitachi (Japan).
- UV-Visible spectrophotometer, Agilent 8453 (USA).
- Zetasizer, Nano – Z, Malvern instruments (Oxford, UK).

3.3 Software

Figures were created using the Biorender platform on BioRender.com (2021). All statistical analysis and graphs were performed using Graphpad Prism version 8 (La Jolla California, USA). Statistical significance among the groups was determined via two-sample student *t*-test and one-way ANOVA analysis. Dunnett's test were utilized for multiple comparisons. The data are expressed as mean ± standard deviation (SD), n=3. The results are reported as statistically significant when $p < 0.05$.

4 METHOD

4.1 Preparation of zwitterionic nanoparticles

Preparation of DNA nanogel and antimicrobial loading

The preparation of DNA nanogel was done by following a two-step annealing method, previously reported (with some slight modifications) (107) using three DNA nanostructures (Y-SAF, Y-SAB, L-SAC) (**Figure 7**). Briefly, stochiometric concentrations of each DNA sequence were mixed with 10 µL 1x diluted encapsulation buffer (EB) and ultrapure pure water to achieve a total volume of 100 µL of the desired nanostructures.

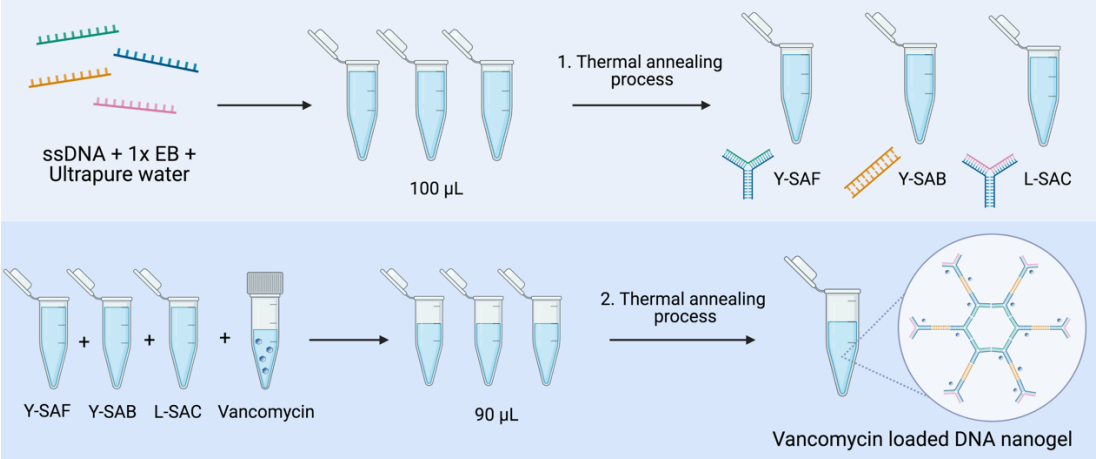

Figure 7: *Fabrication of vancomycin loaded DNA nanogels via pre-loading method.*

The concentrations of the individual nanostructures were as follows: 4 µM Y-SAF, 1 µM Y-SAB and 6.5 µM L-SAC. The samples were hybridized in a thermal cycler to form the DNA nanostructures via the thermal annealing process. Y-SAF samples and L-SAC samples had the same annealing conditions of: 95°C for 5 minutes, 60 °C for 30 minutes, 50 °C for 30 minutes, 37 °C for 30 minutes, 25 °C for 30 minutes and 4 °C for another 3 ½ h. Whereas Y-SAB had the following conditions: 95 °C for 30 minutes, 55 °C for 30 minutes, 37 °C for 30 minutes, 25 °C for 20 minutes and 4 °C for 3 ½ h. Fifteen µL of each nanostructures were subsequently combined with 45 µL vancomycin (final concentration of 1.28 mg/mL) to achieve the vancomycin loaded DNA nanogel or with buffer to achieve the blank DNA nanogel respectively. The samples were then hybridized via a second annealing process under the

conditions of 95 °C for 5 minutes, 25 °C for 30 minutes and then 4 °C for 3 ½ h to obtain the self-assembled DNA nanogels.

Preparation of liposomes

Preparation of liposomes were done using the standard thin-film hydration method (**Figure 8**). In brief, pure soy phosphatidylcholine (SPC) (Lipoid S100), 1.2-Dioleyloxy-3-dimethylaminopropane (DODMA) and PEG3-mannose (mannose) or Cholesteryl hemisuccinate (CHEMS) were dissolved sequentially in a round-bottom flask with methanol.

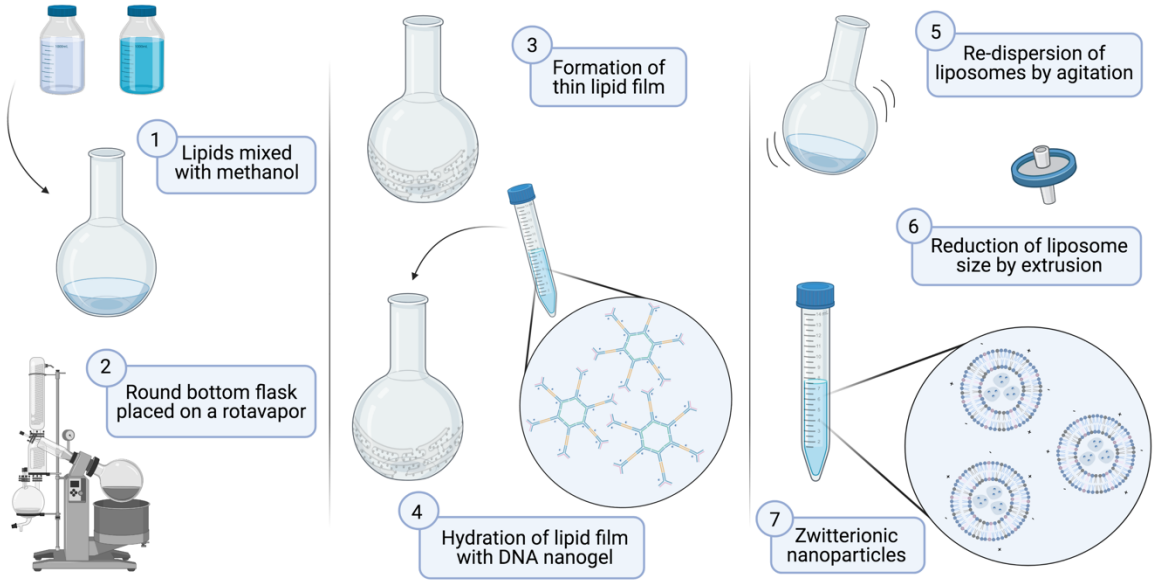

Figure 8: *Fabrication steps of zwitterionic nanoparticles.*

The solution were then gently mixed and placed on a rotary evaporator with a pressure and rotation speed of 60 mmHg and 60 rpm, respectively. The water bath held a constant temperature of 45 °C to develop the lipid film for 1 h. Afterwards, the lipid film was rehydrated with the DNA nanogel solution. To obtain defined sized liposomes the solution were extruded 5 times through a polycarbonate membrane with pore size of 800 nm, then repeated with 400 nm membrane and 200 nm, respectively. The formulation samples were stored at 4 °C until needed. The following table present the zwitterionic nanoparticles lipid mole percentage composition (**Table 3**).

Table 3: Lipid composition of the zwitterionic nanoparticles.

Formulation	P (mol %)	D (mol%)	M (mol%)	C (mol%)
PD (95/5)	95	5	-	-
PDM (92.5/5/2.5)	92.5	5	2.5	-
PDM (90/5/5)	90	5	5	-
PDC (92.5/5/2.5)	92.5	5	-	2.5
PDC (90/5/5)	90	5	-	5
PDC (85/5/10)	85	5	-	10

P: *Soy phosphatidylcholine* (SPC) ; **D**: *1.2-Dioleyloxy-3-dimethylaminopropane* (DODMA) ; **M**: *16:0 PA-PEG3-mannose* ; **C**: *Cholesteryl hemisuccinate* (CHEMS).

4.2 Characterization

Hydrodynamic diameter, polydispersity and zeta potential measurements

The hydrodynamic diameter (size), poly dispersity index (PDI) and zeta potential of the formulations were determined using the Zetasizer (Nano-z, Malvern instruments) via dynamic light scattering (DLS) technique. A cuvette containing a 100x dilution of formulation in 1x EB buffer was prepared for the size and size distribution measurements. For the zeta potential measurements, a capillary cell containing 50x dilution of the formulation in filtered tap water was used. The cell was cleaned with the same sample solution prior to use. Size, PDI and zeta potential was monitored over time to also assess the stability of the zwitterionic nanoparticles. Three replicates were obtained from each sample measurement and the average reading recorded as mean ± standard deviation (SD).

Morphology of zwitterionic nanoparticles

The morphology of the nanoparticles was investigated by transmission electron microscopy (TEM). The formulation was diluted 100x and 50x with deionized water and 5 μL was pipetted onto mesh carbon grids and left to adsorb for 5 minutes. Afterwards, 5 μL of the contrast solution, UranyLess, was added and allowed to stain the grid for 40 seconds. Then, the grids

were washed with deionized water and allowed to dry for an addition of 20 minutes prior to imaging. The samples were imaged using TEM (HT7800, Hitachi).

Determination of entrapment efficiency %

The entrapment efficiency (EE %) was evaluated using the dialysis bag method and the samples quantified with the UV-spectrophotometer. Dialysis bags with molecular cut-off at 12-14 kDa were used to dialyze 500 µL of formulation sample in a beaker containing 50 mL of 1x EB buffer. The formulation was allowed to sit for 4 h at room temperature. Thereafter, the remaining volume of formulation in the dialysis bags was determined, and 80 µL of the dialyzed formulation (or non-dialyzed formulation) was vortex and disrupted with 720 µL methanol. Removal of the DNA nanostructures was done using centrifugal filter units, and the samples were centrifuged at 13 000 rpm for 2 minutes. The absorbance of the flow through solution containing vancomycin was then measured using the UV-spectrophotometer. The entrapment efficiency of vancomycin was then calculated based on the absorbance values using a pre-obtained calibration curve. The following equation was used to calculate the entrapment efficiency:

$$EE\ \% = \frac{C_{encap}}{C_{total}}\ x\ 100\ \%$$

4.3 Biofilm sensitivity and binding

Lipopolysaccharide effect on formulation

To study the interactions between the formulation and biofilm matrix, Alexa fluor 594 stained lipopolysaccharide (LPS) was chosen as a model component of the EPS. Changes in the fluorescence intensity of LPS in the presence of varying concentrations of the zwitterionic nanoparticles was assessed through recording changes in fluorescence. Prior to experiments with formulation, a reference fluorescent curve of the LPS (0.25, 0.5, 1 and 2 µg/mL) was obtained using the microplate reader (Spark, Tecan). Thereafter, serial dilutions of the nanoparticle formulation ranging from 25x to 1600x of the stock was prepared and mixed with the LPS (final concentration of 4 µg/mL) to find the most optimal formulation dilution. Hundred µL of the nanoparticle formulation was combined with 100 µL of the LPS solution.

An amount of 50 μL of the mixture was then added to a costar black 96-well plate, and for the negative and positive controls, 1x EB buffer or DNA nanogels were used respectively. The most optimal formulation dilution was determined to be 50x and therefore used in the following experiments. The experiments were performed at both neutral pH and acidic pH values (pH 7.4 and pH 5.5). All experiments were performed in triplicates and the results reported as mean ± SD.

Dextran effect on formulation

Similarly, the interaction between dextran (another component of the EPS) and formulation was also assessed by recording the changes in fluorescence. The optimized PDM 90/5/5 formulation was chosen for further assessment. A reference fluorescence peak curve of dextran was also obtained between 0.25, 0.5, 1 and 2 μM. A final concentration of 1 μM dextran was added to serial dilutions of the formulation (25x – 1600x), whereas 1x EB buffer served as the negative control. Triplicate volumes of the samples were added in a costar black 96-well plate and the fluorescence intensity was measured in plate reader (Spark, Tecan).

Zwitterionic nanoparticle responsiveness

To assess the sensitivity of the formulation to enzymes (i.e. lipase) or toxins (i.e. α-hemolysin) produced by biofilms, changes in the size of the nanoparticles was analyzed using Zetasizer (Nano-Z, Malvern instruments) in the presence of either lipase or α-hemolysin. Lipase (0.5, 1, 2, and 8 mg/mL) or α-hemolysin (75, 150 and 300 nM) was added to a diluted solution of the nanoparticle (100x) and the sample was measured at 0 h, 1 h, 2 h, 5 h and 24 h. Three replicates were obtained for each measurement.

4.4 *In vitro* drug release

The *in vitro* drug release of vancomycin from the nanoparticle formulation was assessed using a multi-station Franz diffusion cell system. Briefly, the system was heated to 35 °C and the 5 mL equipped receptor chambers were filled with phosphate buffered saline (PBS) at pH 7.4 under constant stirring using a magnetic stir bar. Prior to use, fitted cellophane membranes were cut out and submerged into deionized water for 5-10 minutes, then the membranes were

sandwiched between the receptor chamber and donor chamber. Thereafter, 700 μL of the formulation was loaded into the donor cell. To examine the influence of bacteria enzyme on the drug release profile, the formulations were added to the donor cell with lipase at final concentration of 1, 4 or 8 mg/mL. The donor chamber was then sealed with rubber plug and parafilm.

Sampling of the released antibiotic into the receptor chamber was taken after 1 h, 2 h, 4 h, 8 h, 12 h and 24 h. The receptor chambers were refilled with 500 μL buffer after each sampling to ensure continuous sink condition. At the end of the experiment, the remaining formulation in the donor chamber was collected into a 2 mL centrifuge tube. The amount of drug released at each timepoint was then quantified via absorbance readings with the UV-spectrophotometer and reported as the percentage mean ± SD from duplicate readings in reference to the total amount of drug loaded in the formulation prior to the start of the experiment. The following equation was used to calculate the cumulative drug release percentage:

$$Cumulative\ drug\ release\ \% = \frac{Weight\ of\ drug\ released\ (\mu g)}{Theoretical\ drug\ amount\ in\ formulation}\ x\ 100\ \%$$

4.5 Biofilm studies

Biofilm inhibition experiments

To evaluate the ability of the vancomycin loaded zwitterionic nanoparticles to inhibit biofilm formation, a fluorescently labelled *S. aureus* strain (NCTC 8325 pCM29 green fluorescent (GFP)) was grown in the presence or absence of the nanoparticles. For the bacterial work, 10 mL of nutrient tryptic soy broth (TSB) (supplemented with chloramphenicol 10 μg/mL) was inoculated with the bacteria and incubated overnight (37 °C, 100 rpm). The optical density (OD) of the overnight culture was then adjusted to 0.07 (10^8 colony forming units (CFU)/mL). The exact concentration of vancomycin was determined via absorbance readings obtained via UV-spectrophotometer and compared with the calibration curve. Serial dilutions of the formulation was prepared in TSB growth medium to give a final desired concentration range of vancomycin from 0.5 to 32 μg/mL. To grow the biofilms, the diluted formulations were supplemented with 12.5 % $^{w}/_{v}$ glucose stock (final concentration of 1% $^{w}/_{v}$) and the bacteria solution (10^6 CFU). Aliquots of 200 μL were separately loaded in quadruplicates into the 96-

well plate and incubated for 24 h at 37 °C. As a control, 1x EB buffer was used. After 24 h, the biofilm growth solution was replaced with fresh media and the fluorescence reading taken using microplate reader (Spark, Tecan) at an excitation and emission wavelengths of 480 nm and 530 nm, respectively.

Biofilm eradication experiments

To assess biofilm eradication, biofilms were grown as described above without the zwitterionic nanoparticles i.e. with 12.5 % $^{w}/_{v}$ glucose (final concentration of 1 % $^{w}/_{v}$) and the bacteria solution (10^6 CFU). Aliquots of 200 μL of the solutions were added to the 96-well plate and incubated at 37 °C for 6 h. After biofilm development, the growth media was gently discarded via a vacuum tube and replaced with 100 μL of formulation to give a final vancomycin concentration of 1, 5, 10, 50, 100 and 500 μg/mL. The 96-well plate was then incubated at 37 °C. After 24 h, the biofilms were quantified via fluorescent changes using the microplate reader and crystal violet staining.

Crystal violet stain

Crystal violet 0.1% $^{w}/_{v}$ stain was prepared from a 1% $^{w}/_{v}$ crystal violet stock solution to further assess the biofilm mass. Thereafter, 125 μL of crystal violet was added to the biofilms and stained for 10 minutes. The solutions were then discarded and the wells were washed with filtered tap water to remove the excess dye. Photographic images were then taken using a digital camera. To solubilize the dye and resuspend the biofilms, 200 μL dimethyl sulfoxide (DMSO) was added into each well. The solubilized biofilm solutions were further diluted 4x by adding 50 μL of the solution to an addition of 150 μL DMSO in new wells. Absorbance readings was obtained at 590 nm using a microplate reader (Spark, Tecan). The experiment was carried out in triplicates.

SEM imaging of biofilm

To visualize the antibiofilm effect of the formulations and changes to the morphology of the bacteria, scanning electron microscopy (SEM) was performed. The biofilms were grown as abovementioned without the nanoparticles on poly-l-lysine coated coverslips. The coverslips

were added to 12-well plate and aliquots of 1 mL of the growth solution (growth media containing glucose 12.5 % $^{w}/_{v}$ and 10^6 CFU bacteria solution) was added to the wells. The plate was incubated at 37 °C. After 6 h, the growth solution was replaced with 1 mL of formulation to give a final vancomycin concentration of 1, 5, 10 and 50 μg/mL. Growth media only served as negative control. Prior to imaging, the sample on the coverslips were washed twice using 1 mL sterile PBS. Then, 4 % formaldehyde in addition to 2.5 % glutaraldehyde (in PBS) was added to each coverslip to fix the samples. Thereafter, the slides were placed in a refrigerator overnight at 4 °C. After incubation, the samples were washed twice with 500 μL PBS and the coverslips stained with 1% osmium tetraoxide (OsO_4) for 30 minutes. Afterwards, the OsO_4 was discarded and fresh water was added to the slides for 5 minutes. The staining and addition of water was then repeated. Ethanol series of 30 % for 5 minutes, 60 % for 10 minutes, 90 % for 10 minutes and 100 % for 10 minutes was used to dehydrate the samples prior to drying in critical point dryer (EM CPD300, Leica) and sputter coating with gold and palladium (Polaron Range Sputter Coater, Quorom Technologies Ltd). The samples were imaged using SEM (Sigma, Zeiss).

Biofilm penetration assay

Evaluation of the ability of the zwitterionic nanoparticles to bind and penetrate into the *S. aureus* biofilms was investigated using confocal laser scanning microscopy (CLSM). GFP labeled *S. aureus* biofilms were grown as previously described, in 8 well chambered coverslips for 24 h. Fluorescently labelled PDM 90/5/5 formulations (PDM^{Rho}) were prepared with the addition of 18:1 Liss Rhod PE. After growing the biofilms for 24 h, the growth solution was discarded and the biofilms were treated with 300 μL of 50 μg/mL PDM^{Rho} 90/5/5 formulation at pH 5.5 for a duration of 30 minutes or 120 minutes. Prior to imaging, the biofilms were washed with sterile water to remove unbound nanoparticles on the biofilm surface. Thereafter, the biofilm bound zwitterionic nanoparticles were observed under CLSM with excitation and emission wavelengths of 480 nm and 530 nm (GFP) and of 560 nm and 583 nm (rhodamine B), respectively.

4.6 Cell culture

Cytotoxicity of zwitterionic nanoparticles

The cell toxicity of the formulations was assessed using human immortal keratinocytes, HaCaT cells. The cells were cultured in medium cell culture flasks with Dulbecco's Modified Eagle's Medium (DMEM) high glucose (supplemented with 10 % $^{w}/_{v}$ fetal bovine serum (FBS) and 1% penicillin-streptomycin). At 80% confluency, the cell monolayer was washed twice with 10 mL of phosphate-buffered saline (PBS). The PBS was discarded, then 3-4 mL of PBS + EDTA (0.25 mM) was added to remove cell to cell adhesion and the flask was incubated for 10 minutes. Thereafter, 1 ml of 0.25 % trypsin was added and further incubated for 2 minutes to detach the cells. The cell solution was then added to 7 mL of fresh DMEM and the solution pipetted to separate the cells. The cell density was measured using a handheld automated cell counter device. Afterwards, 200 µL of the cell solution was seeded at a cell density of 6000 cells per well in a 96-well plate. The plates were incubated for 24 h at 37 °C. The cytotoxicity of the formulation was determined at final vancomycin concentrations of 0.5, 1, 5, 10 and 50 µg/mL. The exact concentration of vancomycin in the formulation was determined using a UV-spectrophotometer prior to cytotoxicity assays. Wells containing only DMEM solution served as a negative control and free vancomycin served as a positive control. From each sample concentration, 100 µL was added into 4 wells, and the plates were incubated for another 24 h. The cytotoxicity of the formulation was determined by 3-(4.5-dimethylthiazol-2-yl)-2.5-diphenyltetrazoliumbromide (MTT) assay.

MTT studies

The colorimetric MTT assay was used to investigate the cytotoxicity of formulation on HaCaT cells. Briefly, tetrazolium salt was weighed and ultra-pure water was added to achieve a stock concentration of 5 mg/mL. From this stock, a 10x dilution of MTT in DMEM (0.5 mg/mL) was prepared and used in the experiment. The test agents from each well were discarded, then 200 µL of the 10x diluted MTT solution was added and incubated for 2-4 h. After incubation, the MTT solution was removed, and 100 µL of DMSO was added into each well to dissolve the formazan crystals. Investigation of the cell viabilities and quantification of formazan was done by microplate reader (Spark, Tecan).

4.7 *Ex vivo* pig skin biofilm eradication model

The biofilm eradication efficacy of the zwitterionic nanoparticles was further assessed using an *ex vivo* pig skin model previously reported (with some slight modifications) (119). Sections of pig ear skins of 5 mm were cut using a circular biopsy punch. The skin sections were transferred to a 24-well plate and thoroughly washed 3 times with sterile water. To disinfect the skins, 500 µL of chloramphenicol (10 µg/mL) was used to treat the sections for 1 h. After disinfection the skin sections were washed 3 times with PBS and incubated with 500 µL of 70 % ethanol for 20 minutes to ensure sterility. Afterwards, the sections were washed 3 times with PBS and incubated in PBS. After 1 h, the skin sections were transferred with the skin side up to a 96-well plate containing 150 µL solidified agar to ensure hydration of the skin. The skins were allowed to dry for 15 minutes prior to addition of 20 µL bacteria solution of *S. aureus* (equivalent to 10^6 CFU). The plate was incubated at 37 °C for 24 h to establish mature biofilms. Then, 50 µL of the formulation was added to the skin sections and the plate was again incubated for an additionally 24 h. For the negative control, 1x EB buffer was applied to the skin sections. Additionally, skin sections without any bacteria and treatment was also prepared for the adjustment of the fluorescence baseline. PBS was added to the empty wells to keep the skins well hydrated and to minimize evaporation. Post-incubation, the sections were transferred to a costar black 96-well plate and the fluorescence changes were measured in microplate reader (Spark, Tecan). The experiments were done in triplicates.

5 RESULTS AND DISCUSSION

In this study, a pH responsive nanocarrier was fabricated as a strategy to improve the performance of antimicrobials against biofilm infections. To achieve this, vancomycin loaded DNA nanogels (Van-DNs) were coated with a lipid layer prepared from varying the mole percentage of Soy phosphatidylcholine (SPC), 1.2-Dioleyloxy-3-dimethylaminoproane (DODMA) and Cholesteryl hemisuccinate (CHEMS) or 16:0 PA-PEG3-mannose (mannose) to form a series of zwitterionic nanoparticles from which the optimal system with ideal pH responsiveness was determined (**Figure 9**).

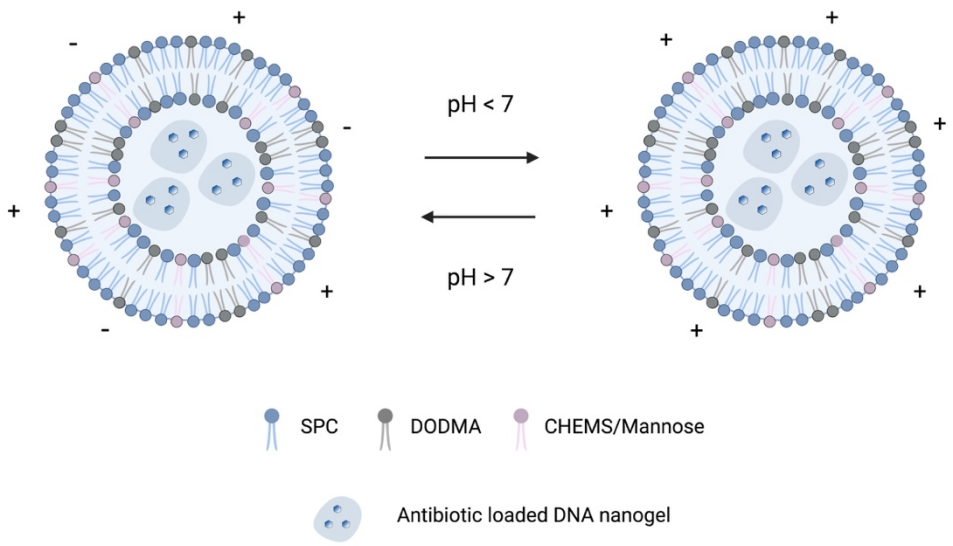

Figure 9: *Schematic illustration of the zwitterionic nanoparticle with surface modulation to achieve pH responsiveness.*

We hypothesized that the optimal system could sustain the release of vancomycin, improve drug specificity and binding affinity to bacterial biofilms as well as retain antibiofilm efficacy.

5.1 Characterization

Effect of lipid composition on the pH responsiveness of the nanoparticles

First, blank DNs were prepared and coated with varying proportions of the individual lipids as presented in **Table 2** using approximately 7.5 – 7.8 mg/mL total lipid concentration. Using zeta potential measurements at different pH conditions, we examined the effect of the lipid compositions on the surface potential of the formulations. Also termed electrokinetic potential, the zeta potential reflects the potential difference between the electric double layer of an electrophoretically mobile particle and the layer of dispersant around them (77). Generally, the dispersal of a charged anionic particle creates an adsorbed double layer on its surface. This layer (i.e. the electric double layer) consists of a strongly adhered stern layer (with cations) and a diffusion layer (with both cations and anions) (120, 121). As the outermost layer, the composition of the diffusion layer is highly variable and is dependent on several factors such as the pH and ionic strength of the dispersant (77). The pH of the dispersant is highly relevant in pharmaceutical formulations and is described as the most influential parameter in zeta potential measurement given its influence on stability/flocculation of pharmaceutical products. Specifically, when the pH of a colloidal formulation (e.g. liposomes) is close to its isoelectric point, the colloidal system loses its stability and agglomerates (77). Since we sought to prepare a zwitterionic formulation with good stability at acidic pH so as to enhance uptake into the biofilm, the choice of the lipid is very important. Using an ionizable lipid with improved stability at low pH was therefore warranted.

As shown in **Figure 10A**, the PD 95/5 formulation demonstrated the most positive zeta potential as predicted (+27.03 ± 0.45 mV at pH 7.3 and +40.53 ± 0.74 mV at pH 4.2), due to the highly cationic nature of the ionizable lipid, DODMA. In keeping the mole percentage of DODMA, constant, we reduced the ratio of the neutral SPC lipid since it played a negligible role on the surface charge of the formulation and incorporated the anionic lipids to prepare the PDM (mannose) or PDC (CHEMS) formulations. At lower concentration of 0.25 mM, the PDM formulation with mole percentage of 92.5/5/2.5 presented a positive zeta potential of +12.83 ± 0.16 mV at pH 7.3 and +31.2 ± 0.17 mV at acidic pH (pH 4.2) (**Figure 10A**). Since this system was not optimal, we increased further the concentration of the mannose to 0.5 mM. Zeta potential measurements of PDM 90/5/5 revealed a close to neutral surface potential of -6.67 ± 0.07 mV at pH 7.3 with a sharp reversal to a cationic value of +12.33 ± 0.51 mV at acidic pH.

This reduced zeta potential is attributed to the increased concentration of the anionic mannose which neutralizes the positive charge of DODMA.

In reciprocating the abovementioned mole percentages, the PDC formulations were prepared. At mole percentages of 92.5/5/2.5 and 90/5/5, the PDC formulations both presented a positive zeta potential of +20.80 ± 0.15 mV and +13.80 ± 0.46 mV, respectively at physiological pH (pH 7.6). At acidic pH, a significant increase in the zeta potential to +40.8 ± 0.65 mV (PDC 92.5/2.5/2.5) and +41.17 ± 0.25 mV (PDC 90/5/5) was observed. Compared to the PDM 90/5/5, the PDC 90/5/5 formulation exhibited a more drastic switch in charge at acidic pH (i.e. a charge change of ~ +26 mV was seen for the PDC formulations compared with a charge change of ~ +19 mV for the PDM formulations). This is attributable to the ionizable cationic DODMA in corporation with CHEMS, whose surface is highly affected by pH. Seeking to completely neutralize the zeta potential of the PDC formulations, PDC 85/5/10 was prepared with a more negative zeta potential of –10.4 ± 0.54 mV at pH 7.6. Despite the increment of the mole percentage of CHEMS in the PDC formulation the observed change in zeta potential at pH 4.5 resulted in a charge switch to +37.6 ± 0.17 mV which was almost similar to the other PDC formulations (**Figure 10B**).

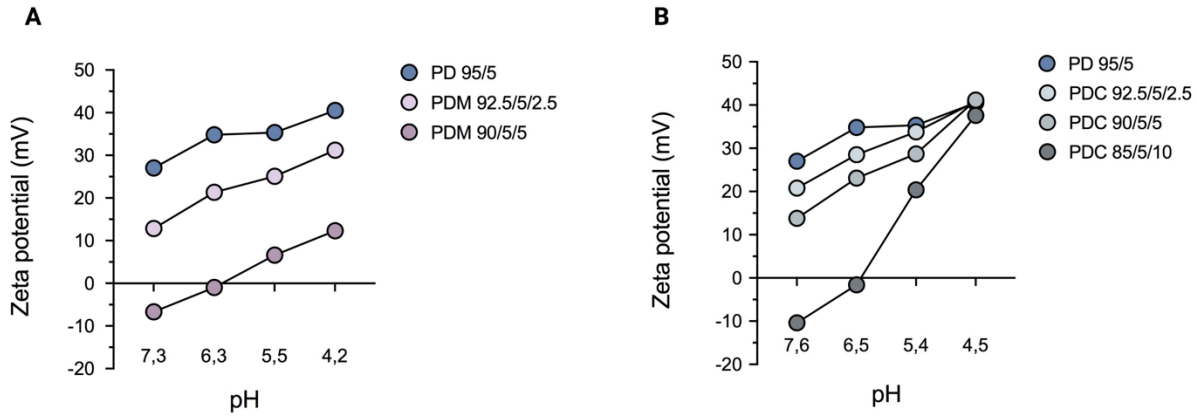

Figure 10: *Effect of lipid compositions and pH on zeta potential in A) PDM formulations and B)PDC formulations.*

We propose that this observation can be attributed to the reversal of CHEMS within the formulation from a lamellar phase at physiological pH to a hexagonal phase (head group inverted state) at acidic pH (122). This change influences the surface potential of the PDC

formulation and allows the overall charge to be dominated by the DODMA lipid. Unlike the PDC formulation, the PDM retains its lamellar phase wherein the exposed anionic head group from the mannosylated lipid neutralizes part of the charge from DODMA to significantly reduce the zeta potential at acidic pH. Therefore, despite utilizing a higher mole percentage of the anionic component (CHEMS) to neutralize the surface charge in the PDC formulation, at acidic pH, the anionic head group is inverted and does not contribute to the surface potential. Consequently, we believed that the PDM 90/5/5 formulation exhibited the most optimal pH responsiveness due to the lower mole percentage requirements. Thus, to compare the zwitterionic properties, the PDC formulation with similar mole percentage as the PDM formulation was chosen for further evaluation. However, since the PDC 90/5/5 formulation presented cationic values at both physiological and acidic pH, the PDC 85/5/10 formulation was also utilized as a control for the optimized PDM 90/5/5 formulation.

Size and zeta potential characterization of the nanoparticles

When designing nanocarriers, adequate characterization of the physiochemical property of the nanoparticle is essential for the development of well-defined and pertinent DDS. Properties such as size and surface charge play a major role in the ability of a nanosystem to succeed since they influence many aspects such as nanoparticle stability, interaction with targets, accumulation, toxicity and clearance from the body (123). The size of the nanoparticles is often expressed as radius or hydrodynamic diameter. Due to the small sizes of the nanoparticles, their surface-to-volume ratio is higher compared to larger objects which consequently increases the total surface area and makes the nanoparticles potentially more reactive i.e. imparts higher magnetic and conductivity properties (124). The size range of nanoparticles is often broad and was defined in 2011 by the European Commission (125) to be between 1 – 100 nm for ≥ 50% of the particles. However, this definition is only a recommendation and should be used as a reference for identification of nanoparticles. In reality, larger nanoparticles have been prepared and reported to exhibit good efficacy while presenting advantages such as increased drug loading capability and reduced premature clearance by the renal excretion system. Therefore, the optimal nanoparticle size highly depends on the therapeutic application route and desired site of action (126).

The encapsulation of drugs in liposomes has been shown to improve the therapeutic efficacy of antimicrobials in skin therapies (127). Compared to conventional formulations, liposomes

provide improved absorption, increased penetration rates and have enhanced the local concentration of the drugs that accumulate in the skin. In addition to lipid composition and lamellarity, the size of the liposome is a crucial factor that influences the observed enhancement of skin therapies (128). Considering this, du Plessis and colleagues suggested that liposomes of 200 nm – 300 nm were the optimum size range for the topical drug delivery of drugs (129). Furthermore, the size can also affect the bacteria and biofilm interactions (130). For instance, Meers and colleagues demonstrated that liposomal amikacin nanoparticles of ~300 nm size penetrated into *P. aeruginosa* biofilm and infected mucus more readily, whereas larger beads (1000 nm) in comparison did not (131). In this project, we therefore sought to prepare nanoparticles with a size range of 200-250 nm to ensure co-encapsulation of the nucleic acid nanostructures and antibiotic without compromising biofilm penetration. We included the nucleic acid within the formulation as a previously published study by Obuobi and colleagues (107) demonstrated that the entrapment of nucleic acid imparted anti-inflammatory activity and improved the loading efficacy of vancomycin.

Following the assessment of the effect of the lipid compositions on pH responsiveness of the zwitterionic nanoparticles, DLS experiments were conducted in order to investigate and characterize the size, size distribution and zeta potential of the formulations. The PDC 90/5/5, PDC 85/5/10 and PDM 90/5/5 formulations were evaluated and compared to the PD 95/5 controls. As shown in **Figure 11A**, the size of the PDM 90/5/5 and PDC 90/5/5 were ~200 nm at physiological pH. PDC 90/5/5 and PDM 90/5/5 achieved sizes of 221.73 ± 0.93 nm and 220.63 ± 0.84 nm respectively, which was significantly larger than the PD 95/5 formulation (183.03 ± 1.23 nm). This observation is potentially due to the electrostatic repulsion between the polyanionic DNA and the anionic lipids in PDM and PDC formulations. Conversely, the PDC 85/5/10 formulation displayed an even larger size of 250.13 ± 2.53 nm. A further hypothesis for the increased size of PDC 85/5/10 formulation is due to poor entrapment of the DNA nanogel, increasing the variation of liposome size. As presented in **Figure 11B**, all of the nanoparticles exhibited a low polydispersity index (PDI) of 0.17 ± 0.01 (PD 95/5), 0.22 ± 0.01 (PDC 90/5/5) and 0.20 ± 0.02 (PDM 90/5/5), indicating a homogenous and narrow size distribution of the liposomes (**Figure 11D**). However, the PDC 85/5/10 formulation presented a higher PDI of 0.43 ± 0.003, indicating a higher degree of multimodal size distribution (data presented in **Appendix Figure 1**). For lipid-based DDS, a PDI value > 0.3 is usually undesired and considered as unacceptable (132).

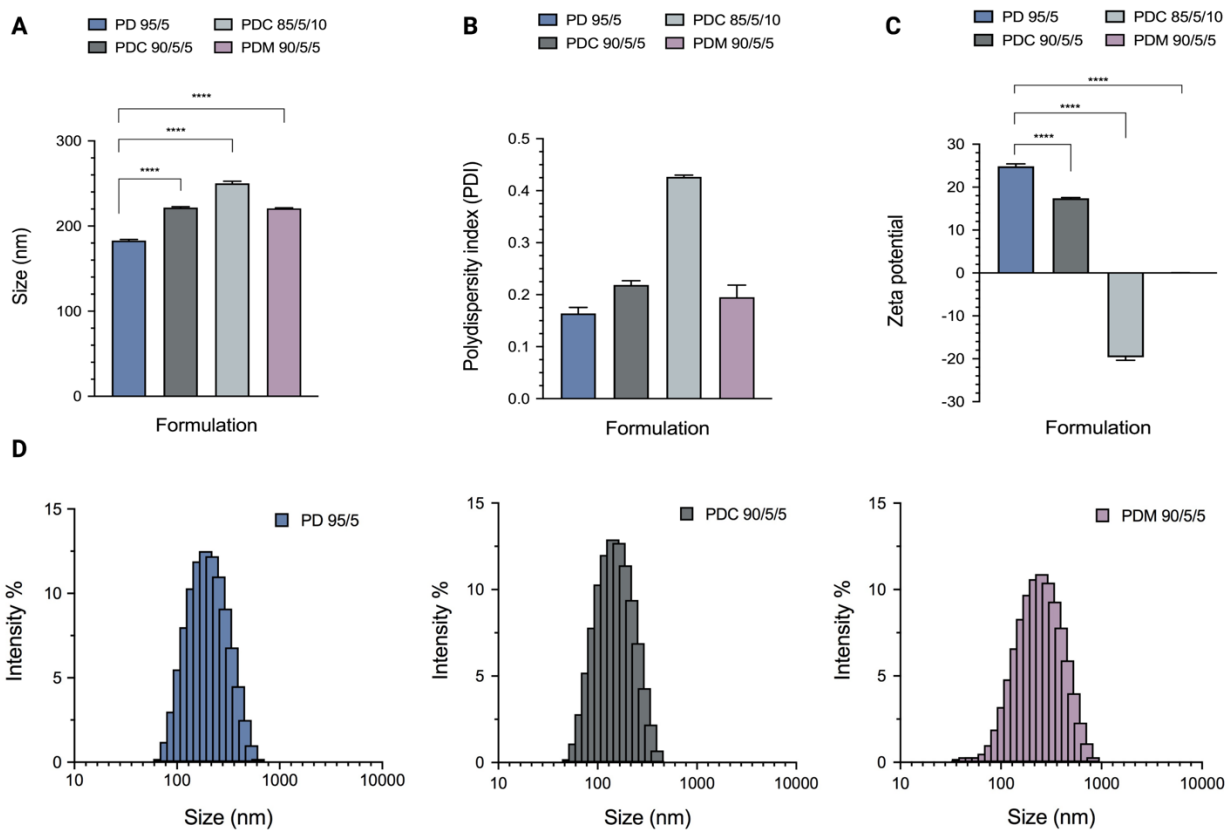

Figure 11: *DLS measurements of the different zwitterionic formulations A) size, B) PDI, C) zeta potential and D) size distribution. Values based on mean ± SD (n=3).*

Zeta potential measurements (**Figure 11C**) for the PDC 90/5/5 was +17.40 ± 0.17 mV at pH 7.4 compared to PDM 90/5/5 which revealed a neutral charge of 0.02 ± 0.02 mV. Given the observed neutral charge of the PDM 90/5/5 and its retained pH responsiveness, the PDM 90/5/5 formulation was identified as the optimal formulation with the ideal surface charge properties. PDC 90/5/5 was further used for comparison, while the PDC 85/5/10 formulation was not investigated any further due to its larger size and PDI value.

Effect of biofilm-mimicking pH conditions on formulation characteristics

Next, to further investigate the pH effect on the different zwitterionic nanoparticles, size and zeta potential measurements were obtained both at pH 7.4 and pH 5.5. By varying the acidic conditions of the formulations, changes in pH may influence the overall size of the nanocarriers. As shown in **Figure 12A**, both the PD 95/5 and the PDM 90/5/5 maintained their size at reduced pH levels, showing no significant changes. On the other hand, the PDC 90/5/5 formulation

showed a significant increment from 221.73 ± 0.93 nm (PDI: 0.22 ± 0.008) at pH 7.4 nm to 233.17 ± 0.93 nm (PDI: 0.23 ± 0.014) at pH 5.5. Additionally, the PDC 90/5/5 demonstrated an altered intensity and size distribution at pH 5.2 after 24 h (**Appendix Figure 2**), whereas the PDM 90/5/5 formulation exhibited a similar intensity in size distribution at pH 7.2 and pH 5.2 (**Appendix Figure 3**). This observation is potentially due to the protonation of carboxyl group of CHEMS under acidic milieu. This weakens the interactions between the complementary lipid anionic CHEMS and DODMA to potentially promote liposome fusion and destabilization to cause aggregation. Similar findings were observed by Sudimack and colleagues, when oleyl alcohol liposomes composed of CHEMS, egg phosphatidylcholine (PC) and Tween-80 incubated in pH 5.0 demonstrated a time and pH-dependent increase in particle size, where up to 15-fold increase in size was observed (133).

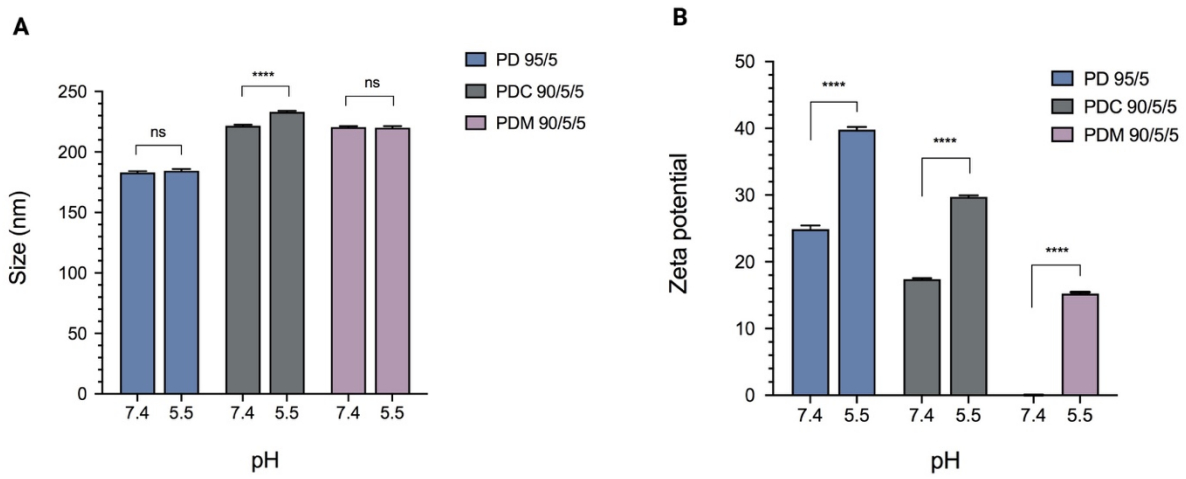

Figure 12: *Effect of pH on A) size and B) zeta potential of formulations. Values based on mean ± SD, n=3.*

As presented in **Figure 12B**, the zeta measurements of the zwitterionic nanoparticles revealed the ability of both anionic lipids (i.e. CHEMS and mannose) to lower the positive baseline charge of PD at physiological pH. As compared to the CHEMS modified formulations, the incorporation of mannose lowered the surface charge of the PD to a much higher extent at physiological pH. The formulations exhibited zeta potentials of +24.87 ± 0.55 mV (PD 95/5), +17.4 ± 0.17 mV (PDC 90/5/5) and +0.02 ± 0.02 mV (PDM 90/5/5) at physiological pH, switching to +39.77 ± 0.42 mV (PD 95/5), +29.73 ± 0.21 mV (PDC 90/5/5) and +15.23 ± 0.21 mV (PDM 90/5/5) at acidic pH, making the increment in zeta potential somewhat similar (~15

mV) for the different nanoparticles. However, only the PDM 90/5/5 zwitterionic nanoparticle presented a neutral surface charge at physiological pH.

Although formulations with zeta potential greater than -30 mV or +30 mV has been shown to have better colloidal stability, and therefore could possibly reduce the aggregation effect (77), formulations with higher cationic charge have also been reported to possess higher toxicity (78, 79). Concordantly, the PDM 90/5/5 formulation which exhibited neutral charge at physiological pH demonstrated the most suitable surface properties as previously described. Additionally, the subtle positive charge observed at lowered pH level could possibly reduce the toxicity of the PDM 90/5/5 formulation compared to the PD 95/5 and PDC 90/5/5 formulations, which is highly desired to maintain good biocompatibility.

Stability of the formulations

The stability of the formulations is an important parameter that guides prediction of the quality of formulations. Changes such as aggregation are detrimental to the zwitterionic formulations and can be attributed to leakage of the entrapped nucleic acid nanogel and/or the cargo (134). Stability studies of the formulation was therefore monitored over time via changes in size and zeta potential over 4 weeks at 4 ºC to investigate the absence of aggregation.

As shown in **Figure 13A,** the size of the formulations were stable after 2 weeks. After 4 weeks, no relevant increase in the size of the nanoparticles was observed. Conversely, the zwitterionic nanoparticles revealed a reduction in the hydrodynamic size for both the PDC 90/5/5 and PDM 90/5/5 formulations. For instance a reduction in the size of the PDM 90/5/5 formulation from 220.63 ± 0.84 nm to 204.57 ± 1.56 nm was observed. Nevertheless, with an approximate size of 200 nm, the formulation was deemed suitable for topical application as reported in literature. While zeta potential values lower than -30 mV and higher than +30 mV can indicate better colloidal stability for nanoparticles as abovementioned, stability is seldom determined on zeta potential only, but are also highly dependent on forces such as wan der Waals and electrostatic repulsion (77).

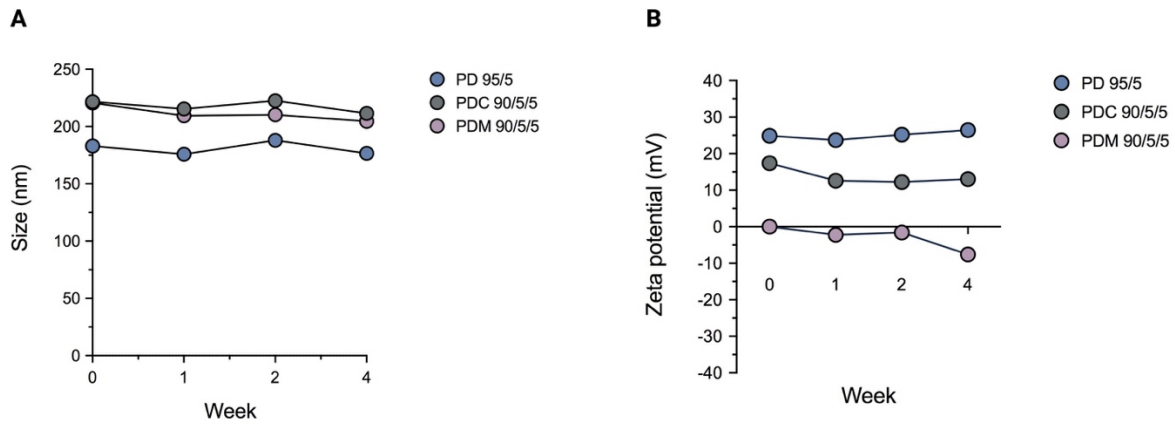

Figure 13: *Stability of formulations monitored via A) size and B) zeta potential changes over 4 weeks. Values based on mean, n=3.*

Accordingly, colloidal systems with zeta potential between -30 mV to + 30 mV could still demonstrate high stability. Zeta potential measurements of the formulations revealed a drop in zeta potential for the PDM and PDC formulations (**Figure 13B**). After 4 weeks, a change in zeta from +0.02 ± 0.02 mV to -7.61 ± 0.78 mV was observed for the PDM 90/5/5 formulations. Similarly, the PDC formulations revealed a zeta from +17.4 ± 0.17 mV to +13.03 ± 0.32 mV demonstrating somewhat maintained surface charge and overall stability.

Morphology of the zwitterionic nanoparticles

In addition to size and surface characterization, the shape of the nanocarriers is also a determining factor than can influence the fate of the nanocarrier in the body (135). For instance, Gratton and colleagues investigated the impact of nanoparticle shape on cellular uptake. They reported that rod-shaped nanoparticles displayed the most optimal uptake, followed by spherical, cylindrical and cube nanoparticles (136). Moreover, rod-like silica nanoparticles designed by Slomberg and coworkers demonstrated improved ability to eradicate *S. aureus* and *P. aeruginosa* biofilms, whereas spherical shaped nanoparticles were much less effective (137). Considering topical application, deformable liposomes which have the ability to adapt their deformability and shape due to incorporation of edge activators, have been shown to enhance the skin permeation compared to conventional liposomes (138). Tak and colleagues investigated the ability of differently shaped silver nanoparticles to penetrate skin in both *in vitro* and *in vivo* models. The *in vivo* studies using mice showed that the rod-shaped

nanoparticles exhibited better penetration and accumulation in the blood compared to spherical and triangular shaped nanoparticles (139).

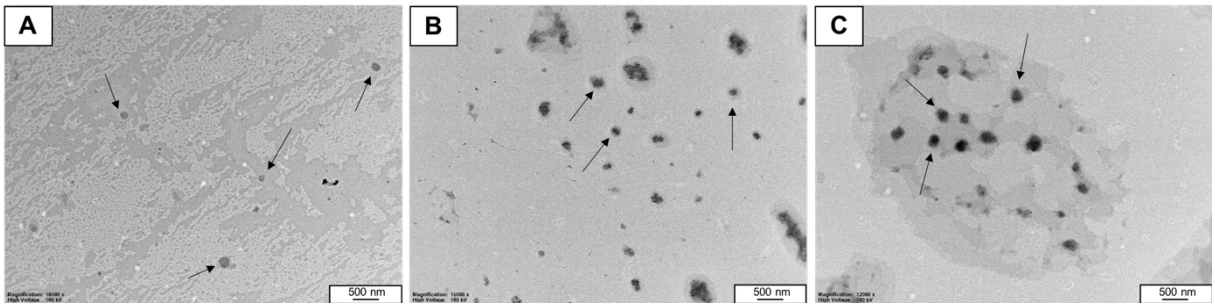

Figure 14: *Morphology of zwitterionic nanoparticles A) PD 95/5 B) PDC 90/5/5 and C) PDM 90/5/5 using TEM (scalebar: 500 nm).*

To further correlate the DLS measurements, the morphology of the nanoparticles was investigated using transmission electron microscopy (TEM). As indicated in **Figure 14**, all the three formulations displayed a spherical shape. Comparative analysis of the visual appearance of the PD 95/5 formulation revealed a smaller size than the PDM 90/5/5 and the PDC 90/5/5 formulation. This observation is in good agreement with the results obtained from the DLS analysis.

Entrapment efficiency (EE%) of the zwitterionic nanoparticles

To investigate the impact of mannose modification on the entrapment of vancomycin, EE% measurements of PDM 90/5/5 formulation and PDC 90/5/5 were compared to the PD 95/5 formulation. As shown in **Figure 15**, the entrapment of vancomycin in the formulations was comparable and modification with the anionic lipids did not influence the loading of vancomycin.

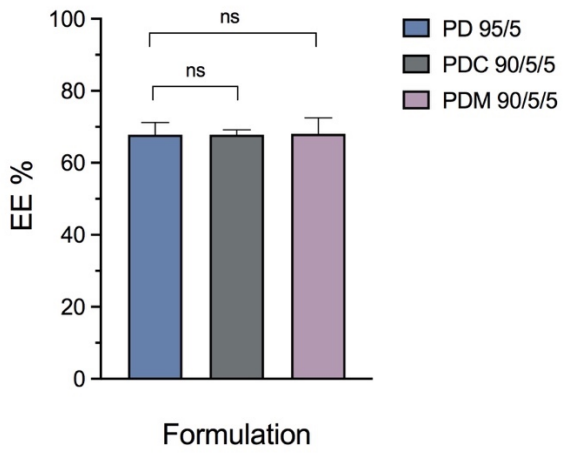

Figure 15: *Entrapment efficiency % of formulations, values based on mean ± SD, n=2.*

Specifically, PDM 90/5/5 exhibited an EE% of 68.05 ± 4.45% whereas the PDC 90/5/5 formulation exhibited an EE% of 67.82 ± 1.34% compared to PD 95/5 which displayed 67.8 ± 3.39%. These finding are slightly lower compared to previous work by Obuobi and colleagues, where the EE% of vancomycin in the nucleic acid loaded liposomes was 76.59 ± 3.44% (107). The lower EE% observed for the zwitterionic nanoparticles fabricated in this project can be attributed to the surface modifications with anionic lipids which can compete with vancomycin for electrostatic interaction with the polyanionic DNA and therefore lower the amount of vancomycin interacting with DNA within the core of the liposomes.

5.2 Biofilm sensitivity and binding

Lipopolysaccharide (LPS) and Dextran binding affinity

Lipopolysaccharides (LPS) are bacterial cell wall components which can also be found in the biofilm matrix. In *in vitro* analysis *(140, 141)*, they have been shown to insert into lipid bilayers. The binding affinity of the blank formulations was initially compared with the DNA nanogel (DN) alone by monitoring changes in the fluorescence intensity of LPS at pH 5.5. Thereafter, binding affinity of the formulations was also assessed for the vancomycin loaded nanoparticles.

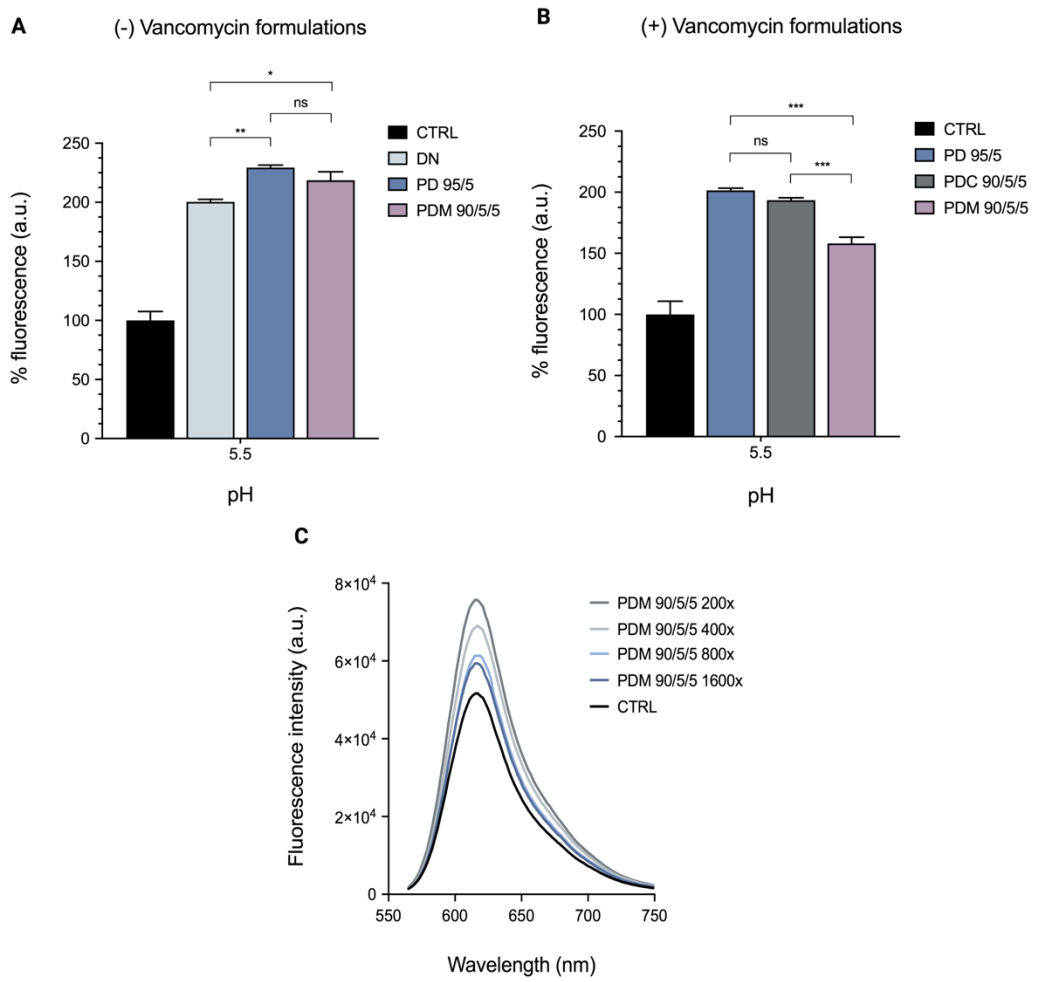

Figure 16*: Binding affinity to LPS to the A) blank formulations and B) formulations with vancomycin. C) Binding affinity of PDM 90/5/5 to dextran. Values based on mean, n=3.*

As shown in **Figure 16A**, the PD 95/5 and PDM 90/5/5 formulations did not compromise the binding affinity of the DNA. On the contrary, DN incorporation resulted in a significant increase of the fluorescence intensity. The observed enhanced fluorescence intensity can be attributed to the synergistic binding affinity of the lipid modified DN compared to the free DN. Following antibiotic incorporation, a significant increased fluorescence intensity was observed for all the three nanoparticles (**Figure 16B**) at pH 5.5. The PD 95/5 formulation showed the greatest fluorescence change 101.54 ± 1.85% compared to the LPS control, followed by the PDC 90/5/5 which recorded a 93.43 ± 1.92% increase in fluorescence and finally, the PDM 90/5/5 formulation which showed an increase of 58.14 ± 5.05%. The observation is in direct correlation with the zeta potential measurements (PD > PDC 90/5/5 > PDM 90/5/5) at acidic pH, therefore we postulate that this interaction is highly dependent on electrostatic interactions. Data from experiments conducted at physiological pH is presented in **Appendix Figure 4**.

Next, binding affinity of the optimized PDM 90/5/5 formulation for polysaccharide components of the biofilm matrix was investigated by monitoring changes in fluorescence intensity of dextran. As shown in **Figure 16C**, in the absence of PDM 90/5/5, the measured fluorescence intensity of dextran was 50534.67 arbitrary units (a.u.). In presence of PDM 90/5/5, a concentration dependent increase in the fluorescence intensity of dextran was observed. For instance, formulations diluted 1600x showed a smaller (14.80 ± 6.45%) increase in the fluorescence intensity compared to 200x diluted formulation (46.41 ± 7.19%). The observed changes in the fluorescence correlate the binding of the PDM 90/5/5 formulations to dextran. Similar to the LPS experiments, we attributed these observations to the electrostatic interaction between the anionic polysaccharide, dextran, and the charged zwitterionic PDM 90/5/5 formulation at acidic pH.

Nanoparticles responsiveness to bacterial enzyme and endotoxin

Several pathogenic bacteria such as *S. aureus* produce enzymes such as lipase which catalyze the hydrolyzation of lipids (142). A myriad of studies have therefore, exploited these inherent enzymes to fabricate nanomaterials with lipase-triggered drug release properties (143, 144). Similarly, the endotoxin α-hemolysin protein is also well-known for its membrane pore-forming ability (145). These molecules therefore provide the potential to stimulate drug release from lipid based nanocarriers for antibacterial therapy. To investigate the sensitivity of the optimized zwitterionic formulation to bacterial toxin and enzyme, changes in size of the formulation PDM 90/5/5 was monitored over 24 h.

As shown in **Figure 17A**, a dose and time dependent degradation of the formulation was observed following exposure to lipase. For instance after 1 h of exposure to 1 mg/mL lipase, a change in the size of the PDM 90/5/5 was observed from 224.27 ± 1.08 nm to 193.5 ± 2.7 nm after 24 h. Upon exposure to higher concentrations of lipase (2 mg/mL and 8 mg/mL) similar time dependent degradation was observed which implies the sensitivity of the nanoparticles to the degradative enzyme.

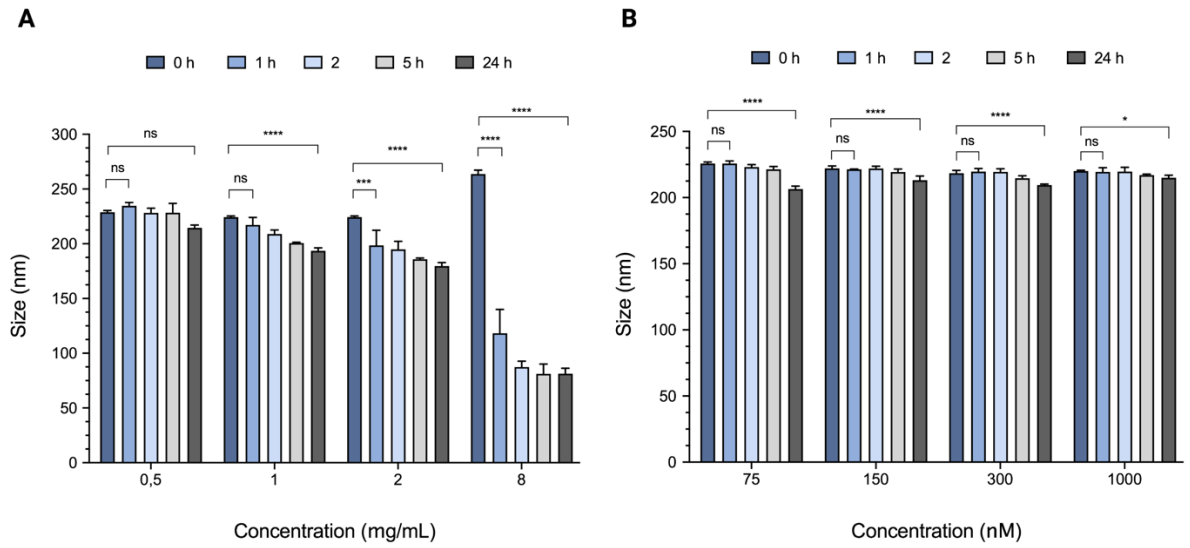

Figure 17: *The responsiveness of PDM 90/5/5 formulation in presence of A) lipase and B) α-hemolysin. Values based on mean, n=3.*

However in the presence of the pore-forming endotoxin α-hemolysin, only a time-dependent degradation of the nanoparticle was observed as shown in **Figure 17B**. For instance, a significant change in the size of the PDM 90/5/5 from 225.77 ± 1.12 nm to 206.4 ± 2.25 nm after 24 h was seen after exposure to 75 nM of the endotoxin. This observation potentially demonstrates a slower and less sensitive effect of the endotoxin on the PDM 90/5/5 formulations which can be attributable to the charge neutralization and reduced access to the bilayer following surface modification. In order to form pores in the liposome bilayer, the interaction of α-hemolysin to lipids is highly dependent on phosphatidylcholine headgroups acting as binding sites on the membrane (146). For instance, Schwiering and colleagues studied the binding affinity of the endotoxin to various liposomes with varying lipid compositions (147). They reported that toxin binding to egg yolk 1.2-diacyl-*sn*-glycero-3-phosphocholine (EPC) was first observed at higher fractions of the lipid, indicating that a certain lipid surface density is needed for sufficient interaction. Additionally, they observed that the binding affinity was higher to sphingomyelin compared to phosphatidylcholine, potentially showing that in order to fully utilize α-hemolysin as a trigger for the drug release, further modifications of the lipid composition is warranted.

5.3 *In vitro* drug release

A crucial requirement necessary to enhance the therapeutic efficacy of the formulations is the ability of the DDS to control the release of entrapped drug cargo as a means to improve the pharmacokinetic profile. As a measure to address this aspect, the design of a formulation which imparts stimuli-responsiveness can possibly prevent premature degradation, sustain the release and increase the bioavailability of the drug locally at desired target site (148). In this study, we sought to leverage on the numerous enzymes (e.g. lipase) present in the biofilm microenvironment to influence and trigger the zwitterionic nanoparticles antimicrobial release. Thus, *in vitro* drug release experiments were conducted to investigate the release profile of vancomycin from the nanoparticles in absence and presence of lipase.

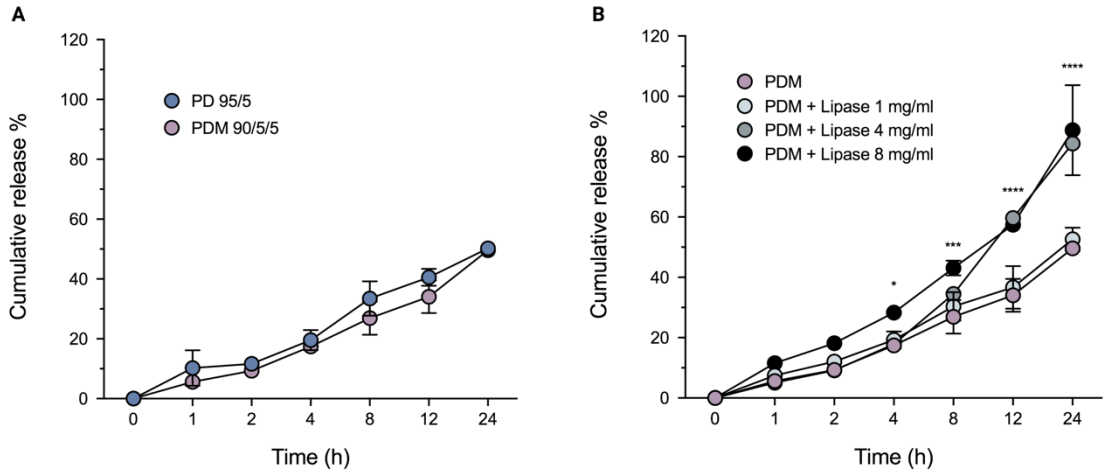

Figure 18: *In vitro drug release of A) PD 95/5 and PDM 90/5/5 and B) PDM 90/5/5 in presence of lipase. Values based on mean ± SD, n=3.*

As shown in **Figure 18A**, PD 95/5 formulation released 40.58 ± 2.85% of vancomycin within 12 h. The total drug release at 24 h was approximately 50.21 ±1.78%. Comparatively, the PDM 90/5/5 formulation released 34.05 ± 5.43% and 49.57 ± 1.46% at 12 h and 24 h, respectively. These observations are similar to previously reported work of Obuobi and colleagues (107), where encapsulation of antibiotic loaded DNA nanogels inside the lipid bilayer structure sustained the release of vancomycin. Moreover, there were no significant changes in the cumulative release from the PDM 90/5/5 formulation compared to the PD 95/5, indicating that mannosylation of the nanoparticles did not significantly influence the release profile.

Next, to investigate the enzyme triggered release profile from the zwitterionic formulation, the PDM 90/5/5 nanoparticle was exposed to different concentrations of lipase (1, 4 and 8 mg/mL) as shown in **Figure 18B**. When exposed to 1 mg/mL of lipase, no difference in the release profile was seen. This can be attributed to reduced degradation of the nanoparticles at low lipase concentrations of 1 mg/mL, as indicated by the slow size reduction obtained by DLS, previously presented in **Figure 17A**. The cumulative release of vancomycin from the nanoparticle increased in presence of 4mg/mL of lipase. At 12 h the cumulative release was 59.67 ± 1.52% and a total of 84.35 ± 1.97% was observed at 24 h, compared to PDM 90/5/5 formulation in absence of lipase at 24 h which exhibited a drastically lower percentage, only reaching 49.57 ± 1.46% after 24 h. Further investigation with 8 mg/mL lipase exhibited a significant increase in the release profile compared to PDM 90/5/5 formulation in absence of lipase. For instance at 4 h, and 24 h the percentage release of the formulation was 57.43 ± 0,78% and 88.76 ± 14.95%, respectively. Surprisingly, the increase of lipase from 4 mg/mL to 8 mg/mL did not significantly affect the cumulative release of vancomycin from the nanoparticle which can indicate that both concentrations encouraged degradation of the bilayer to a similar degree. This could be attributed to substrate saturation, where the addition of enzyme would not necessarily affect the rate of the lipid degradation of the nanoparticle or affect the release profile. These findings correlate with the observed significant reduction in the size upon exposure to high lipase (8 mg/mL) conditions. Additionally, these results demonstrate that the release of vancomycin can be controlled and triggered by lipase, via degradation of the lipid bilayer to contribute to the "on-demand" release of drug.

5.4 Antibiofilm effect

Biofilm inhibition and eradication

Considering the observed release profile from the optimized formulation, we hypothesized that the zwitterionic nanoparticle could preserve the activity of the antimicrobial cargo. Vancomycin is a glycopeptide, which acts by inhibiting the polymerization of growing amino sugars in the peptidoglycan layer in the bacteria cell wall. This antimicrobial is widely used as a first-line agent against severe multidrug-resistant infections caused by Gram-positive bacteria strains, for instance methicillin-resistant *Staphylococcus aureus* (MRSA) (149). Biofilm inhibition and eradication assays were therefore conducted to investigate the ability of the

zwitterionic nanoparticles to prevent and eradicate *S. aureus* biofilms. Vancomycin at 1 μg/mL has previously been reported (107) to completely inhibit the bacteria growth of *S. aureus*. Therefore, we aimed to investigate the antibacterial activity of the formulation at doses based on ½ x MIC – 32x MIC for the biofilm inhibition study.

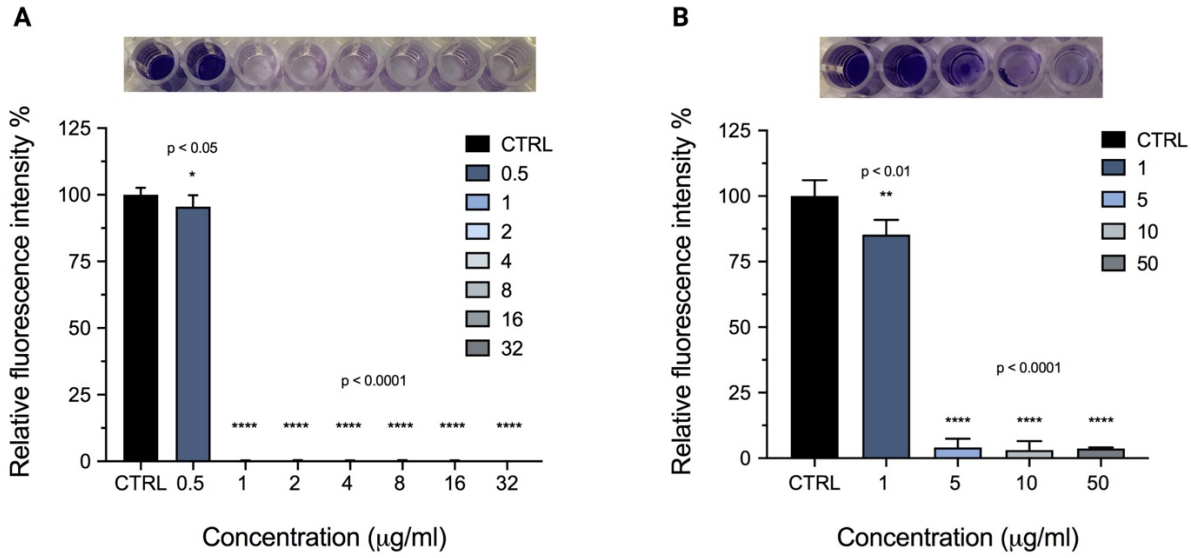

Figure 19: *In vitro antibiofilm activity of PDM 90/5/5 formulation. Effect of formulation on A) biofilm inhibition and B) biofilm eradication. Values based on mean ± SD , n= 3.*

As shown in **Figure 19A**, following treatment with 0.5 μg/mL (1/2x MIC) of vancomycin loaded into the zwitterionic nanoparticles, a significant reduction in biofilm formation was observed with a relative fluorescence intensity of 95.52 ± 4.30% (of fluorescent *S. aureus*) compared to the untreated control group (100%). Exposure to a higher concentration of 1 μg/mL led to a reduced relative fluorescence intensity of 0.31 ± 0.03% of the GFP labelled bacteria, which demonstrates an almost complete inhibition of the biofilm growth at the tested concentrations. To correlate the fluorescence readings, the well-established crystal violet (CV) staining method was performed. Similar to the fluorescence readings, the absence of biofilm mass at concentrations ranging from 1 μg/mL to 32 μg/mL of the vancomycin loaded nanoparticles was observed. For instance at 1 μg/mL, the measured biofilm mass was only 14.97 ± 2.33% (as compared to 100% for untreated control group). These findings indicate that the incorporation of vancomycin into the DN and subsequent exposure to the different thermal hybridization conditions did not degrade the antimicrobial drug. Additionally, it indicates that

the zwitterionic nanoparticles preserved the antimicrobial activity of the drug and released the entrapped cargo when present at targeted bacterial site.

Next, biofilm eradication assays were investigated to determine the ability of the formulations to eradicate 6 h matured biofilms. As shown in **Figure 19B**, at 1 μg/mL of vancomycin loading, a significantly reduced biofilm bioburden was demonstrated with a relative fluorescence intensity of 85.3 ± 5.63%. At higher concentrations of 5 μg/mL, a further improved eradication profile with a relative fluorescence intensity of 4.11 ± 3.34% was observed. The performed CV staining correlated with the abovementioned fluorescence findings, with a drastically reduced biofilm mass of 72.89 ± 2.82% when exposed to 5 μg/mL PDM 90/5/5 as shown in **Figure 19B**.

SEM imaging

The observed biofilm eradication effect of the PDM 90/5/5 formulation was further visualized under SEM. As shown in **Figure 20A**, the untreated control group showed the presence of densely populated bacterial colonies.

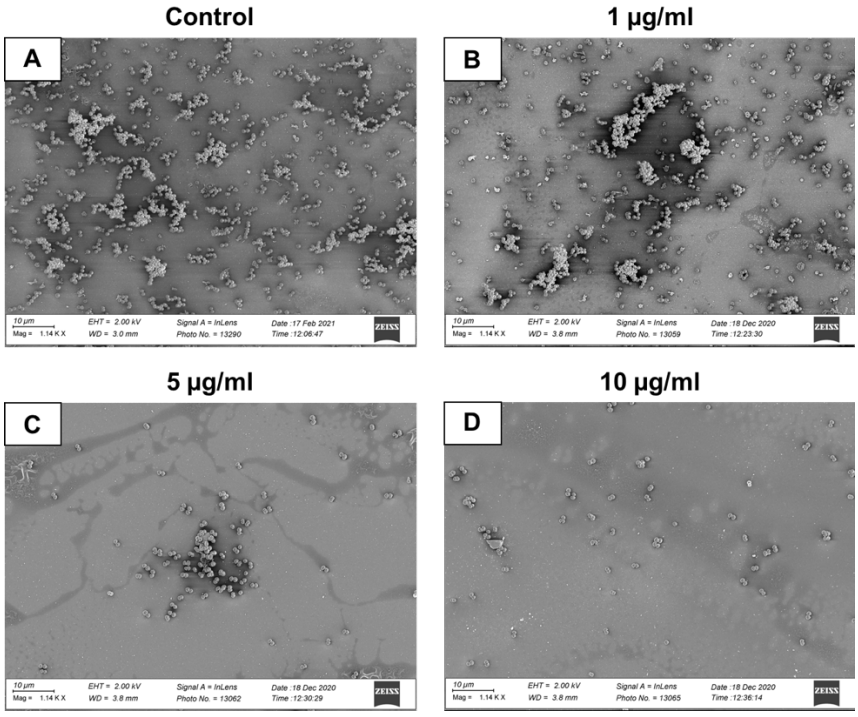

Figure 20: *Effect of A) control, B) 1 μg/mL, C) 5 μg/mL and D) 10 μg/mL PDM 90/5/5 formulation on ultrastructure of S. aureus biofilms using SEM (scalebar: 10 μm).*

Upon addition of 1 μg/mL of the formulation, a small reduction in the density of the bacteria was observed (**Figure 20B**). However, the 5 μg/mL (**Figure 20C**) and 10 μg/mL (**Figure 20D**) treated groups demonstrated a drastic reduction in the density of the bacteria colonies with very few cells present. These results further confirm that the PDM 90/5/5 formulations could sufficiently eradicate biofilms within 24 h.

Biofilm penetration assay

One of the reasons for the many failed treatment of clinical infections is due to the poor bioavailability of antimicrobial drugs. To address this challenge, a DDS which can bind to and penetrate into the layers of the biofilm to deliver the cargo can enhance local drug accumulation within the infection site. Hence, the binding and penetration of the zwitterionic nanoparticles to the biofilm were investigated via CLSM at acidic environment (pH 5.5). As previously described, the sensitivity of the zwitterionic formulations to acidic environment was essential to impart a switch in surface charge of the nanoparticles, from a neutral charge to a cationic charge. As a result, we hypothesized that this will assure binding and penetration through the biofilms. The time dependent penetration of the rhodamine labelled formulations (PDM^{Rho} 90/5/5) was therefore investigated.

As shown in **Figure 21B**, after 30 minutes of exposure to PDM^{Rho} 90/5/5 (50 μg/mL), a weak red fluorescence within the mature *S. aureus* biofilms was observed with a more dominant green fluorescence from the bacteria (GFP).

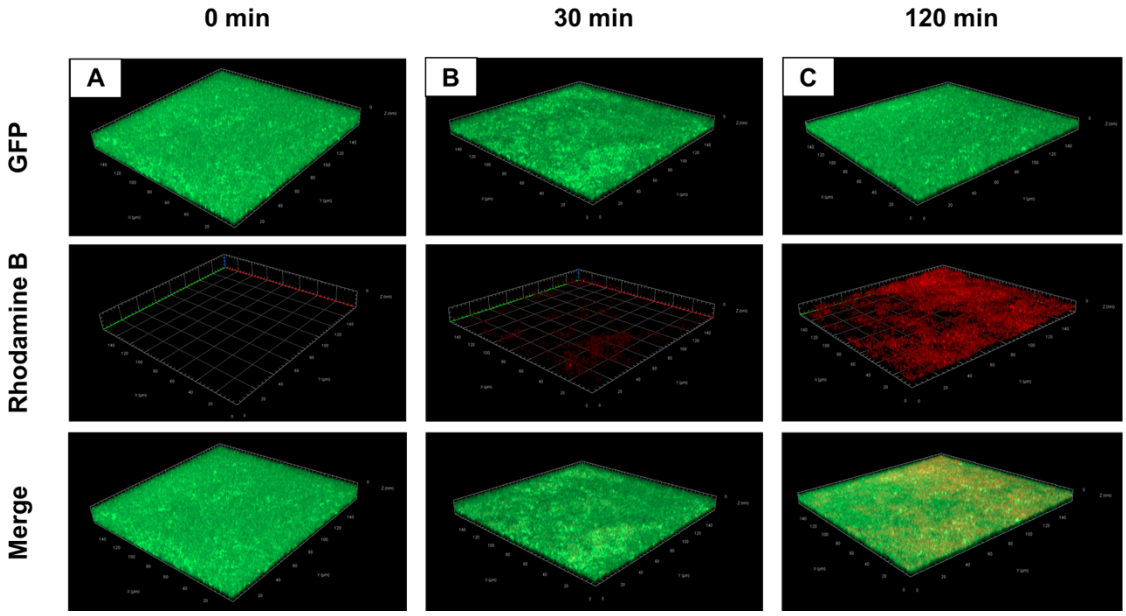

Figure 21: *In vitro biofilm binding and penetration assay toward S. aureus biofilms. CLSM 3D-images of A) CTRL, and after exposure PDM^{Rho} 90/5/5 (50 μg/mL) for B) 30 min and C) 120 min.*

However, after 120 minutes of exposure to the formulation (**Figure 21C**), an increased amount of the red fluorescence from rhodamine B was observed. More importantly, the merged image of the two fluorescence substances showed co-localization of the PDM^{Rho} 90/5/5 (50 μg/mL) with the biofilm which potentially confirms its biofilm uptake. These results confirm the high binding and penetration of the formulation in *S. aureus* biofilms.

5.5 Cytotoxicity

When introducing foreign particles into the human body, toxic substances can possibly induce unwanted immune responses and/or other undesired side effects. There is therefore a great interest to design non-toxic nanocarriers and investigate their biocompatibility as a means to better estimate their ability to integrate with the biological system (150). Hence, the biocompatibility of free vancomycin and vancomycin loaded zwitterionic nanoparticles was evaluated *in vitro* in HaCaT cells.

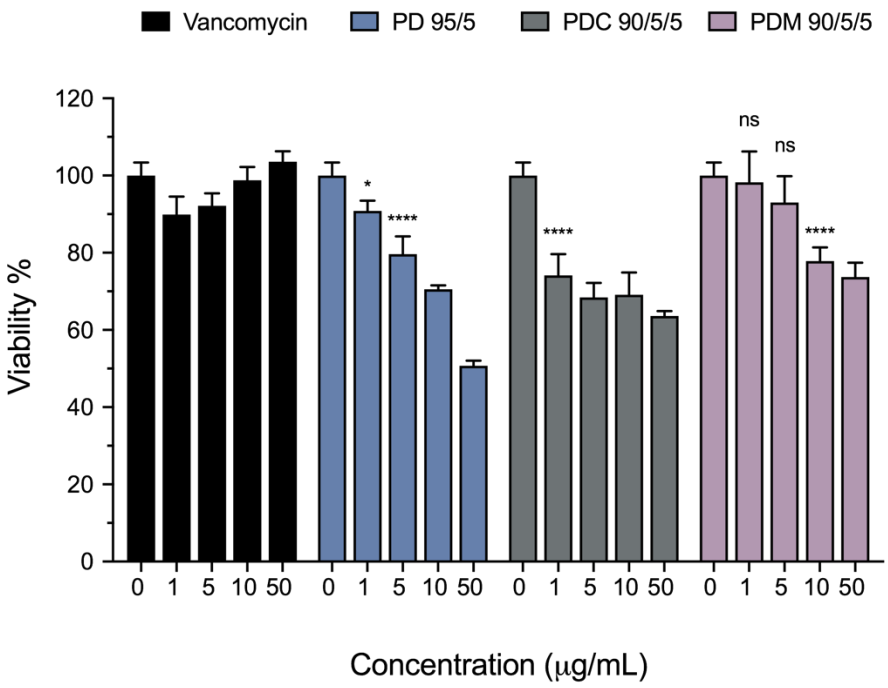

Figure 22: *Cytotoxicity of free vancomycin and formulations with various concentrations assessed on HaCaT cells. Values based on mean ± SD, n=3.*

Free vancomycin at a dose range between 1μg/mL to 50 μg/mL demonstrated negligible toxicity. As shown in **Figure 22**, exposure to 50 μg/mL of PD 95/5 for 24 h resulted in significantly reduced cellular viability of 50.73 ± 1.30% compared to the untreated control group (i.e. 0 μg/mL of PD 95/5). On the other hand, exposure to 50 μg/mL of PDC 90/5/5 resulted in a viability of 63.64 ± 1.25%. According to International Organization for Standardization (ISO) standards (151), a reduced viability less than 70% indicates toxicity, and therefore the PD 95/5 and PDC 90/5/5 formulations demonstrated concentration-dependent toxicity. Conversely, when the cells were exposed to PDM 90/5/5 at the same concentration, the viability exceeded 70% (i.e. 73.72 ± 3.71%), demonstrating reduced toxicity and a good degree of biocompatibility of the formulation towards HaCaT cells. This observation can be attributed to the modulation of the surface potential in the PDM zwitterionic (+0.02 ± 0.02 mV) formulation, compared to the highly cationic PD (+24.87 ± 0.55 mV) and PDC (+17.40 ± 0.17 mV) formulations. As previously mentioned, it is shown that cationic liposomes exhibit greater toxicity compared to neutral or anionic liposomes in some tissue cells (78, 79). Liposomes possessing a higher zeta potential have also been found to be more toxic compared to liposomes with lower zeta potentials (152).

Moreover, the high compatibility of the PDM formulations are in good agreement with previously reported compatibility study of vancomycin loaded DN constructs prepared with neutral SPC liposomes by Obuobi and colleagues (107). In this work, the authors also demonstrated more than 70% cell viability of the vancomycin loaded nucleic acids liposomal hybrids (Van_DNL). In agreement to this study, Ternullo and coworkers utilized the lipid soybean phosphatidylcholine (SPC), to fabricate human epidermal growth factor (heGF) incorporated deformable liposomes for skin therapy (153). The authors observed that the empty neutral liposomes were non-toxic to human foreskin fibroblast (HF) and HaCaT cells after 24 h. Furthermore, after 48 h exposure to the heGF loaded liposomes, the HF proliferation was increased by 40%.

5.6 *Ex vivo* pig skin biofilm eradication

To further assess the translational value of the zwitterionic nanoparticles, the ability of PDM 90/5/5 formulations to eradicate biofilms caused by GFP labelled *S. aureus* was investigated in an *ex vivo* porcine explant model (**Figure 23A**).

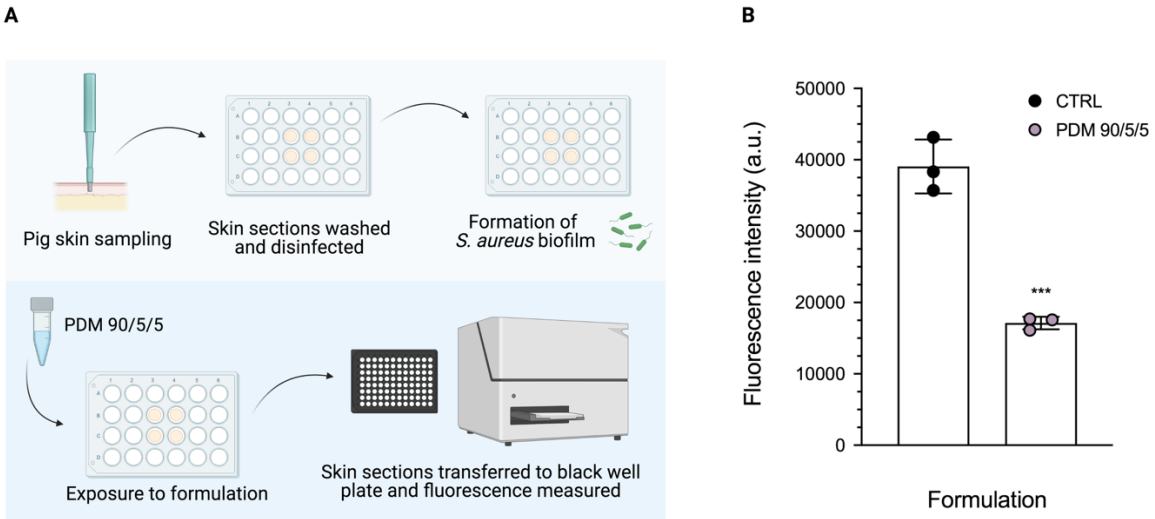

Figure 23: *Ex vivo porcine skin explant biofilm eradication model and effect of the PDM 90/5/5 formulation on an ex vivo wound infection model. A)Schematic illustration of experimental steps to establish the model. B) Fluorescence intensity results. Data calculated based on baseline adjustment and presented as mean ± SD as well as individual values, n= 3.*

As shown in **Figure 23B**, in the control group (treated with 50 µL 1x EB buffer) a fluorescence intensity of 3779.13 a.u. was observed after 24 h following biofilm establishment. However, a significant reduction in fluorescence intensity on the skin sections was observed when 50 µL of the PDM 90/5/5 formulation was topically applied once, as compared to the untreated control group. This resulted in a fluorescence change of 56.16 ± 2.26% and indicates the ability of the formulation to reduce bacterial burden within 24 h. These findings correlates with the pre-reported *in vitro* results and revealed the antimicrobial potency of the PDM 90/5/5 formulation as well as demonstrates their potential as an effective antimicrobial delivery system in topical wound therapy.

6 CONCLUSION

The main aim of this study was to design a zwitterionic nanocarrier system to enhance the delivery of antimicrobial drugs against *S. aureus* wound biofilms. To achieve this, we sought to fabricate a pH and enzyme responsive DDS to better control the behavior of the nanocarrier (i.e. enhanced biofilm binding, control drug release and minimize toxicity).

A successful fabrication of the zwitterionic nanoparticle PDM 90/5/5 was achieved. Characterization by DLS and TEM presented well-formed zwitterionic nanoparticles with the desired surface characteristics (i.e. size, shape, surface charge) and the formulation exhibited good stability over one month. Entrapment efficiency studies revealed that the modulation of the lipid surface did not compromise the loading of the drug. Further evaluations demonstrated the sensitivity of the formulations to components of the biofilm matrix (i.e. LPS, dextran), bacterial enzyme (i.e. lipase) and endotoxin (i.e. α-hemolysin). *In vitro* drug release experiments demonstrated enhanced release in presence of lipase, indicating the enzyme triggered and controlled release properties of the formulation. Antibiofilm properties of the formulation was assessed by crystal violet staining method, SEM imaging, CLSM and by an *ex vivo* porcine pig skin model, which showed the ability of the formulations to bind, penetrate and eradicate *S. aureus* biofilms. Furthermore, the formulation did not possess any significant toxicity towards HaCaT cells.

Although further studies *in vivo* need to be conducted, these findings show the advantageous effect of the surface modification of the liposome to better enhance the therapeutic efficacy of antimicrobial against *S. aureus* biofilms. The PDM 90/5/5 zwitterionic nanoparticle is a promising stimuli responsive DDS, with promising features to address the current burden of clinical biofilm infections on medical devices and chronic wounds. Further optimization of this nanocarrier holds immense promise to combat the current menace of antimicrobial resistance.

7 PERSPECTIVES

The findings from this study opens up new avenues to the previously fabricated nucleic acid loaded liposomal hybrids presented by Obuobi and colleagues (107) in 2020. The current modifications done in this work to develop a nanocarrier with the zwitterionic features is a promising strategy to further improve the efficacy of the designed DDS against biofilms infections. Although the findings from this study provide valuable data, further optimization of the methods and the utilization of broader experimental conditions could be explored. Following are some short and long-term perspectives presented:

- Regarding quantification analysis, utilization of methods and instruments that are more precise could improve the data accuracy. For instance, the use of High Performance Liquid Chromatography (HPLC) for quantification experiments of vancomycin could be done.

- Investigation of size and surface charge characteristics could be explored in simulated biological fluids (e.g. wound exudates) that better mimic *in vivo* bodily fluids to better estimate the effect and potential formation of protein-corona on the liposome surface.

- Investigation of the antibiofilm activity of the formulations against other bacteria strains, for instance different *S. aureus* strains or MRSA.

- Evaluation of the toxicity and biocompatibility of the formulations against other mammalian cells (e.g. fibroblast).

- Optimize the skin conditions in the *ex vivo* porcine skin explant model, to better mimic a real wound infection site with altered physiochemical reactions and utilize human skin sections to evaluate the *ex vivo* efficacy of the formulations.

- Findings from experiments done with our conditions will only be indicative and are not necessary translational to *in vivo* conditions. Therefore, it would be of high interest to further investigate the formulation *in vivo* in fitting animal studies to better evaluate the formulations effect and safety.

8 REFERENCES

1. Tan, S.Y., Tatsumura, Y. (2015). Alexander Fleming (1881-1955): Discoverer of penicillin. *Singapore Medical Journal*. 56(7), 366-367.
2. Ligon, B.L. (2004). Penicillin: its discovery and early development. *Seminars in Pediatric Infectious Diseases.* 15(1), 52-57.
3. Ruddaraju, L.K., Pammi, S.V.N., Guntuku, G.S., Padavala, V.S., Kolapalli, V.R.M. (2020). A review on anti-bacterials to combat resistance: From ancient era of plants and metals to present and future perspectives of green nano technological combinations. *Asian Journal of Pharmaceutical Sciences.* 15(1), 42-59.
4. Zhu, X., Radovic-Moreno, A.F., Wu, J., Langer, R., Shi, J. (2014). Nanomedicine in the Management of Microbial Infection - Overview and Perspectives. *Nano Today*. 9(4), 478-498.
5. Pendleton, J.N., Gorman, S.P., Gilmore, B.F. (2013). Clinical relevance of the ESKAPE pathogens. *Expert Review of Anti-infective Therapy.* 11(3), 297-308.
6. Eleraky, N.E., Allam, A., Hassan, S.B., Omar, M.M. (2020). Nanomedicine Fight against Antibacterial Resistance: An Overview of the Recent Pharmaceutical Innovations. *Pharmaceutics.* 12(2), 1-51.
7. Alberts, B., Bray, D., Hopkin, K., Johnson, A., Lewis, J., Raff, M., *et al*. (2010). Essential cell biology. Introduction to Cells. Garland Science. 11-14.
8. Rang, H.P., Ritter, J.M., Flower, R.J., Henderson, G. (2016). Rang and Dale's Pharmacology. 8th ed: Elsevier Churchill Livingstone. 615-618.
9. Parker, J. (2001). Bacteria. Encyclopedia of Genetics: Academic Press. 146-151.
10. Kapoor, G., Saigal, S., Elongavan, A. (2017). Action and resistance mechanisms of antibiotics: A guide for clinicians. *Journal of Anaesthesiology, Clinical Pharmacology.* 33(3), 300-305.
11. Percival, S.L., McCarty, S.M., Lipsky, B. (2015). Biofilms and Wounds: An Overview of the Evidence. *Advances in Wound Care.* 4(7), 373-381.
12. Vestby, L.K., Grønseth, T., Simm, R., Nesse, L.L. (2020). Bacterial Biofilm and its Role in the Pathogenesis of Disease. *Antibiotics.* 9(2), 1-29.
13. Banerjee, D., Shivapriya, P.M., Gautam, P.K., Misra, K., Sahoo, A.K., Samanta, S.K. (2020). A Review on Basic Biology of Bacterial Biofilm Infections and Their Treatments by Nanotechnology-Based Approaches. *Proceedings of the National Academy of Sciences, India Section B: Biological Sciences.* 90(2), 243-259.

14. Verderosa, A.D., Totsika, M., Fairfull-Smith, K.E. (2019). Bacterial Biofilm Eradication Agents: A Current Review. *Frontiers in Chemistry.* 7, 1-17.
15. Singh, N., Romero, M., Travanut, A., Monteiro, P.F., Jordana-Lluch, E., Hardie, K.R., *et al.* (2019). Dual bioresponsive antibiotic and quorum sensing inhibitor combination nanoparticles for treatment of Pseudomonas aeruginosa biofilms in vitro and ex vivo. *Biomaterials Science.* 7(10), 4099-4111.
16. Zhang, Y., Pi, Y., Hua, Y., Xie, J., Wang, C., Guo, K., *et al.* (2020). Bacteria responsive polyoxometalates nanocluster strategy to regulate biofilm microenvironments for enhanced synergetic antibiofilm activity and wound healing. *Theranostics.* 10(22), 10031-10045.
17. Donlan, R.M., Costerton, J.W. (2020). Biofilms: survival mechanisms of clinically relevant microorganisms. *Clinical Microbiology Reviews.* 15(2), 167-193.
18. López, D., Vlamakis, H., Kolter, R. (2010). Biofilms. *Cold Spring Harbor Perspectives in Biology.* 2(7), 1-11.
19. Rutherford, S.T., Bassler, B.L. (2012). Bacterial quorum sensing: its role in virulence and possibilities for its control. *Cold Spring Harbor Perspectives in Medicine.* 2(11), 1-25.
20. Mukherjee, S., Bassler, B.L. (2019). Bacterial quorum sensing in complex and dynamically changing environments. *Nature Reviews Microbiology.* 17(6), 371-382.
21. Sharma, D., Misba, L., Khan, A.U. (2019). Antibiotics versus biofilm: an emerging battleground in microbial communities. *Antimicrobial Resistance and Infection Control.* 8, 1-10.
22. Davies, D.G., Geesey, G.G. (1995). Regulation of the alginate biosynthesis gene algC in Pseudomonas aeruginosa during biofilm development in continuous culture. *Applied and Environmental Microbiology.* 61(3), 860-867.
23. Becker, P., Hufnagle, W., Peters, G., Herrmann, M. (2001). Detection of differential gene expression in biofilm-forming versus planktonic populations of Staphylococcus aureus using micro-representational-difference analysis. *Applied and Environmental Microbiology.* 67(7), 2958-2965.
24. Xiu, W., Gan, S., Wen, Q., Qiu, Q., Dai, S., Dong, H., *et al.* (2020). Biofilm Microenvironment-Responsive Nanotheranostics for Dual-Mode Imaging and Hypoxia-Relief-Enhanced Photodynamic Therapy of Bacterial Infections. *Research.* 1-15.

25. Zhou, Z., Hu, F., Hu, S., Kong, M., Feng, C., Liu, Y., *et al.* (2018). pH-Activated nanoparticles with targeting for the treatment of oral plaque biofilm. *Journal of Materials Chemistry B.* 6(4), 586-592.
26. Foulston, L., Elsholz, A.K.W., DeFrancesco, A.S., Losick, R. (2014). The Extracellular Matrix of *Staphylococcus aureus* Biofilms Comprises Cytoplasmic Proteins That Associate with the Cell Surface in Response to Decreasing pH. *mBio.* 5(5), 1-9.
27. Tan, Q., Ai, Q., Xu, Q., Li, F., Yu, J. (2018). Polymorphonuclear Leukocytes or Hydrogen Peroxide Enhance Biofilm Development of Mucoid Pseudomonas aeruginosa. *Mediators of Inflammation.* 1-14.
28. Jang, I-A., Kim, J., Park, W. (2016). Endogenous hydrogen peroxide increases biofilm formation by inducing exopolysaccharide production in Acinetobacter oleivorans DR1. *Scientific Reports.* 6(1), 1-12.
29. Gough, D.R., Cotter, T.G. (2011). Hydrogen peroxide: a Jekyll and Hyde signalling molecule. *Cell Death and Disease.* 2(10), 1-8.
30. Preiser, J-C. (2012). Oxidative Stress. *Journal of Parenteral and Enteral Nutrition.* 36(2), 147-154.
31. Fux, C.A., Costerton, J.W., Stewart, P.S., Stoodley, P. (2005). Survival strategies of infectious biofilms. *Trends in Microbiology.* 13(1), 34-40.
32. James, G.A., Swogger, E., Wolcott, R., Pulcini, Ed., Secor, P., Sestrich, J., *et al.* (2008). Biofilms in chronic wounds. *Wound Repair and Regeneration.* 16(1), 37-44.
33. Zhao, G., Usui, M.L., Lippman, S.I., James, G.A., Stewart, P.S., Fleckman, P., *et al.* (2013). Biofilms and Inflammation in Chronic Wounds. *Advances in Wound Care.* 2(7), 389-399.
34. Sorsa, T., Tjäderhane, L., Salo, T. (2004). Matrix metalloproteinases (MMPs) in oral diseases. *Oral Diseases.* 10(6), 311-318.
35. McCarty, S.M., Cochrane, C.A., Clegg, P.D., Percival, S.L. (2012). The role of endogenous and exogenous enzymes in chronic wounds: A focus on the implications of aberrant levels of both host and bacterial proteases in wound healing. *Wound Repair and Regeneration*. 20(2), 125-136.
36. Fulaz, S., Vitale, S., Quinn, L., Casey, E. (2019). Nanoparticle–Biofilm Interactions: The Role of the EPS Matrix. *Trends in Microbiology.* 27(11), 915-926.
37. Anderl, J.N., Franklin, M.J., Stewart, P.S. (2000). Role of antibiotic penetration limitation in Klebsiella pneumoniae biofilm resistance to ampicillin and ciprofloxacin. *Antimicrobial Agents and Chemotherapy.* 44(7), 1818-1824.

38. Brooun, A., Liu, S., Lewis, K. (2000). A dose-response study of antibiotic resistance in Pseudomonas aeruginosa biofilms. *Antimicrobial Agents and Chemotherapy.* 44(3), 640-646.

39. Bagge, N., Ciofu, O., Skovgaard, L.T., Høiby, N. (2000). Rapid development in vitro and in vivo of resistance to ceftazidime in biofilm-growing Pseudomonas aeruginosa due to chromosomal β-lactamase. *APMIS*. 108(9), 589-600.

40. Dhar, N., McKinney, J.D. (2007). Microbial phenotypic heterogeneity and antibiotic tolerance. *Current Opinion in Microbiology.* 10(1), 30-38.

41. Ceri, H., Olson, M.E., Stremick, C., Read, R.R., Morck, D., Buret, A. (1999). The Calgary Biofilm Device: new technology for rapid determination of antibiotic susceptibilities of bacterial biofilms. *Journal of Clinical Microbiology.* 37(6), 1771-1776.

42. Billings, N., Birjiniuk, A., Samad, T.S., Doyle, P.S., Ribbeck, K. (2015). Material properties of biofilms-a review of methods for understanding permeability and mechanics. *Reports on Progress in Physics.* 78(3), 1-33.

43. Walters, M.C., Roe, F., Bugnicourt, A., Franklin, M.J., Stewart, P.S. (2003). Contributions of antibiotic penetration, oxygen limitation, and low metabolic activity to tolerance of Pseudomonas aeruginosa biofilms to ciprofloxacin and tobramycin. *Antimicrobial Agents and Chemotherapy.* 47(1), 317-323.

44. Stewart, P.S., Costerton, J.W. (2001). Antibiotic resistance of bacteria in biofilms. *The Lancet.* 358(9276), 135-138.

45. Spoering, A.L., Lewis, K. (2001). Biofilms and planktonic cells of Pseudomonas aeruginosa have similar resistance to killing by antimicrobials. *Journal of Bacteriology.* 183(23), 6746-6751.

46. Soares, G.M.S., Figueiredo, L.C., Faveri, M., Cortelli, S.C., Duarte, P.M., Feres, M. (2012). Mechanisms of action of systemic antibiotics used in periodontal treatment and mechanisms of bacterial resistance to these drugs. *Journal of Applied Oral Science*. 20(3), 295-309.

47. Eng, R.H., Padberg, F.T., Smith, S.M., Tan, E.N., Cherubin, C.E. (1991). Bactericidal effects of antibiotics on slowly growing and nongrowing bacteria. *Antimicrobial Agents and Chemotherapy.* 35(9), 1824-1828.

48. Bigger, J. (1944). Treatment of Staphylococcal infections with penicillin by intermittent sterilisation. *The Lancet.* 244(6320), 497-500.

49. Keren, I., Kaldalu, N., Spoering, A., Wang, Y., Lewis, K. (2004). Persister cells and tolerance to antimicrobials. *FEMS Microbiology Letters.* 230(1), 13-18.
50. Keren, I., Shah, D., Spoering, A., Kaldalu, N., Lewis, K. (2004). Specialized persister cells and the mechanism of multidrug tolerance in Escherichia coli. *Journal of Bacteriology.* 186(24), 8172-8180.
51. Roberts, M.E., Stewart, P.S. (2005). Modelling protection from antimicrobial agents in biofilms through the formation of persister cells. *Microbiology Society.* 151(1), 75-80.
52. Smits, W.K., Kuipers, O.P., Veening, J-W. (2006). Phenotypic variation in bacteria: the role of feedback regulation. *Nature Reviews Microbiology.* 4(4), 259-271.
53. Ciofu, O., Rojo-Molinero, E., Macià, M.D., Oliver, A. (2017). Antibiotic treatment of biofilm infections. *APMIS.* 125(4), 304-319.
54. Zaidi, S., Misba, L., Khan, A.U. (2017). Nano-therapeutics: A revolution in infection control in post antibiotic era. *Nanomedicine: Nanotechnology, Biology and Medicine.* 13(7), 2281-2301.
55. Helsedirektoratet. Antibiotika i sykehus - Nasjonal faglig retningslinje (2013). Retrieved from: https://www.helsedirektoratet.no/retningslinjer/antibiotika-i-sykehus (Accessed April 23, 2021).
56. Theuretzbacher, U., Outterson, K., Engel, A., Karlén, A. (2020). The global preclinical antibacterial pipeline. *Nature Reviews Microbiology.* 18(5), 275-285.
57. Patra, J.K., Das, G., Fraceto, L.F., Campos, E.V.R., Rodriguez-Torres, M.D.P., Acosta-Torres, L.S., *et al.* (2018). Nano based drug delivery systems: recent developments and future prospects. *Journal of Nanobiotechnology.* 16(1), 1-33.
58. Bobo, D., Robinson, K.J., Islam, J., Thurecht, K.J., Corrie, S.R. (2016). Nanoparticle-Based Medicines: A Review of FDA-Approved Materials and Clinical Trials to Date. *Pharmaceutical Research.* 33(10), 2373-2387.
59. James, N.D., Coker, R.J., Tomlinson, D., Harris, J.R.W., Gompels, M., Pinching, A.J., *et al.* (1994). Liposomal doxorubicin (Doxil): An effective new treatment for Kaposi's sarcoma in AIDS. *Clinical Oncology*. 6(5), 294-296.
60. Fang, J., Nakamura, H., Maeda, H. (2011). The EPR effect: Unique features of tumor blood vessels for drug delivery, factors involved, and limitations and augmentation of the effect. *Advanced Drug Delivery Reviews.* 63(3), 136-151.
61. Baptista, P.V., McCusker, M.P., Carvalho, A., Ferreira, D.A., Mohan, N.M., Martins, M., *et al.* (2018). Nano-Strategies to Fight Multidrug Resistant Bacteria - "A Battle of the Titans". *Frontiers in Microbiology.* 9, 1-26.

62. Obuobi, S., Škalko-Basnet, N. (2020). Nucleic Acid Hybrids as Advanced Antibacterial Nanocarriers. *Pharmaceutics.* 12(7), 1-25.

63. Liu, Y., Busscher, H.J., Zhao, B., Li, Y., Zhang, Z., van der Mei, H.C., *et al.* (2016). Surface-Adaptive, Antimicrobially Loaded, Micellar Nanocarriers with Enhanced Penetration and Killing Efficiency in Staphylococcal Biofilms. *ACS Nano.* 10(4), 4779-4789.

64. Han, H., Gao, Y., Chai, M., Zhang, X., Liu, S., Huang, Y., *et al.* (2020). Biofilm microenvironment activated supramolecular nanoparticles for enhanced photodynamic therapy of bacterial keratitis. *Journal of Controlled Release.* 327, 676-687.

65. Akbarzadeh, A., Rezaei-Sadabady, R., Davaran, S., Joo, S.W., Zarghami, N., Hanifehpour, Y., *et al.* (2013). Liposome: classification, preparation, and applications. *Nanoscale Research Letters.* 8(1), 1-9.

66. Mozafari, M.R. (2010). Liposomes: Methods and Protocols. Nanoliposomes: Preparation and Analysis. Humana Press. 29-50.

67. Nisini, R., Poerio, N., Mariotti, S,. De Santis, F., Fraziano, M. (2018). The Multirole of Liposomes in Therapy and Prevention of Infectious Diseases. *Frontiers in Immunology.* 9, 1-23.

68. Németh, Z., Pallagi, E., Dobó, D.G., Csóka, I. (2020). A Proposed Methodology for a Risk Assessment-Based Liposome Development Process. *Pharmaceutics.* 12(12), 1-13.

69. Samiei, A., Tamadon, A.M., Samani, S.M., Manolios, N., Sarvestani, E.K. (2014). Engraftment of plasma membrane vesicles into liposomes: A new method for designing of liposome-based vaccines. *Iranian Journal of Basic Medical Sciences.* 17(10), 772-778.

70. Sercombe, L., Veerati, T., Moheimani, F., Wu, S.Y., Sood, A.K., Hua, S. (2015). Advances and Challenges of Liposome Assisted Drug Delivery. *Frontiers in Pharmacology.* 6, 1-13.

71. Couvreur, P., Fattal, E., Andremont, A. (1991). Liposomes and Nanoparticles in the Treatment of Intracellular Bacterial Infections. *Pharmaceutical Research.* 8(9), 1079-1086.

72. Solleti, V.S., Alhariri, M., Halwani, M., Omri, A. (2015). Antimicrobial properties of liposomal azithromycin for Pseudomonas infections in cystic fibrosis patients. *Journal of Antimicrobial Chemotherapy.* 70(3), 784-796.

73. Nicolosi, D., Scalia, M., Nicolosi, V.M., Pignatello, R. (2010). Encapsulation in fusogenic liposomes broadens the spectrum of action of vancomycin against Gram-negative bacteria. *International Journal of Antimicrobial Agents.* 35(6), 553-558.

74. Marier, J-F., Lavigne, J., Ducharme, M.P. (2002). Pharmacokinetics and efficacies of liposomal and conventional formulations of tobramycin after intratracheal administration in rats with pulmonary Burkholderia cepacia infection. *Antimicrobial Agents and Chemotherapy.* 46(12), 3776-3781.

75. Smith, M.C., Crist, R.M., Clogston, J.D., McNeil, S.E. (2017). Zeta potential: a case study of cationic, anionic, and neutral liposomes. *Analytical and Bioanalytical Chemistry.* 409(24), 5779-5787.

76. Wang, D-Y., van der Mei, H.C., Ren, Y., Busscher, H.J., Shi, L. (2020). Lipid-Based Antimicrobial Delivery-Systems for the Treatment of Bacterial Infections. *Frontiers in Chemistry.* 7, 1-15.

77. Bhattacharjee, S. (2016). DLS and zeta potential – What they are and what they are not? *Journal of Controlled Release.* 235, 337-351.

78. Smistad, G., Jacobsen, J., Sande, S.A. (2007). Multivariate toxicity screening of liposomal formulations on a human buccal cell line. *International Journal of Pharmaceutics.* 330(1), 14-22.

79. Dokka, S., Toledo, D., Shi, X., Castranova, V., Rojanasakul, Y. (2000). Oxygen Radical-Mediated Pulmonary Toxicity Induced by Some Cationic Liposomes. *Pharmaceutical Research.* 17(5), 521-525.

80. Radovic-Moreno, A.F., Lu, T.K., Puscasu, V.A., Yoon, C.J., Langer, R., Farokhzad, O.C. (2012). Surface charge-switching polymeric nanoparticles for bacterial cell wall-targeted delivery of antibiotics. *ACS Nano.* 6(5), 4279-4287.

81. Chen, M., Xie, S., Wei, J., Song, X., Ding, Z., Li, X. (2018). Antibacterial Micelles with Vancomycin-Mediated Targeting and pH/Lipase-Triggered Release of Antibiotics. *ACS Applied Materials and Interfaces.* 10(43), 36814-36823.

82. Suk, J.S., Xu, Q., Kim, N., Hanes, J., Ensign, L.M. (2016). PEGylation as a strategy for improving nanoparticle-based drug and gene delivery. *Advanced Drug Delivery Reviews.* 99(Pt A), 28-51.

83. Canaparo, R., Foglietta, F., Giuntini, F., Della Pepa, C., Dosio, F., Serpe, L. (2019). Recent Developments in Antibacterial Therapy: Focus on Stimuli-Responsive Drug-Delivery Systems and Therapeutic Nanoparticles. *Molecules.* 24(10), 1-15.

84. Gao, W., Hu, C-M.J., Fang, R.H., Zhang, L. (2013). Liposome-like Nanostructures for Drug Delivery. *Journal of Materials Chemistry B.* 1(48), 1-35.
85. Zou, P., Stern, S.T., Sun, D. (2014). PLGA/liposome hybrid nanoparticles for short-chain ceramide delivery. *Pharmaceutical Research.* 31(3), 684-693.
86. Zhao, Z., Ding, C., Wang, Y., Tan, H., Li, J. (2019). pH-Responsive polymeric nanocarriers for efficient killing of cariogenic bacteria in biofilms. *Biomaterials Science.* 7(4), 1643-1651.
87. Baillet, J., Desvergnes, V., Hamoud, A., Latxague, L., Barthélémy, P. (2018). Lipid and Nucleic Acid Chemistries: Combining the Best of Both Worlds to Construct Advanced Biomaterials. *Advanced Materials.* 30(11), 1-24.
88. Hu, Q., Li, H., Wang, L., Gu, H., Fan, C. (2019). DNA Nanotechnology-Enabled Drug Delivery Systems. *Chemical Reviews.* 119(10), 6459-6506.
89. Chang, M., Yang, C-S., Huang, D-M. (2011). Aptamer-Conjugated DNA Icosahedral Nanoparticles As a Carrier of Doxorubicin for Cancer Therapy. *ACS Nano.* 5(8), 6156-6163.
90. Mathur, D., Medintz, I.L. (2019). The Growing Development of DNA Nanostructures for Potential Healthcare-Related Applications. *Advanced Healthcare Materials.* 8(9), 1-45.
91. Alberts, B., Bray, D., Hopkin, K., Johnson, A., Lewis, J., Raff, M., *et al.* (2010). Essential cell biology. DNA and chromosomes. Garland Science. 171-178.
92. Watson, J.D., Crick, F.H.C. (1953). Molecular Structure of Nucleic Acids: A Structure for Deoxyribose Nucleic Acid. *Nature.* 171(4356), 737-738.
93. Madhanagopal, B.R., Zhang, S., Demirel, E., Wady, H., Chandrasekaran, A.R. (2018). DNA Nanocarriers: Programmed to Deliver. *Trends in Biochemical Sciences.* 43(12), 997-1013.
94. Seeman, N.C. (1982). Nucleic acid junctions and lattices. *Journal of Theoretical Biology.* 99(2), 237-247.
95. Ding, B., Sha, R., Seeman, N.C. (2004). Pseudohexagonal 2D DNA Crystals from Double Crossover Cohesion. *Journal of the American Chemical Society.* 126(33), 10230-10231.
96. Rothemund, P.W.K. (2006). Folding DNA to create nanoscale shapes and patterns. *Nature.* 440(7082), 297-302.
97. Xu, F., Xia, Q., Wang, P. (2020). Rationally Designed DNA Nanostructures for Drug Delivery. *Frontiers in Chemistry.* 8, 1-13.

98. Ke, Y., Sharma, J., Liu, M., Jahn, K., Liu, Y., Yan, H. (2009). Scaffolded DNA Origami of a DNA Tetrahedron Molecular Container. *Nano Letters.* 9(6), 2445-2447.

99. Bhatia, D., Surana, S., Chakraborty, S., Koushika, S.P., Krishnan, Y. (2011). A synthetic icosahedral DNA-based host–cargo complex for functional in vivo imaging. *Nature Communications.* 2(1), 1-8.

100. Douglas, S.M., Dietz, H., Liedl, T., Högberg, B., Graf, F., Shih, W.M. (2009). Self-assembly of DNA into nanoscale three-dimensional shapes. *Nature.* 459(7245), 414-418.

101. Kwak, M., Herrmann, A. (2011). Nucleic acid amphiphiles: synthesis and self-assembled nanostructures. *Chemical Society Reviews.* 40(12), 5745-5755.

102. Liu, Y., Sun, Y., Li, S., Liu, M., Qin, X., Chen, X., *et al.* (2020). Tetrahedral Framework Nucleic Acids Deliver Antimicrobial Peptides with Improved Effects and Less Susceptibility to Bacterial Degradation. *Nano Letters.* 20(5), 3602-3610.

103. Zhang, Q., Lin, S., Shi, S., Zhang, T., Ma, Q., Tian, T., *et al.* (2018). Anti-inflammatory and Antioxidative Effects of Tetrahedral DNA Nanostructures via the Modulation of Macrophage Responses. *ACS Applied Materials and Interfaces.* 10(4), 3421-3430.

104. Pinheiro, A.V., Han, D., Shih, W.M., Yan, H. (2011). Challenges and opportunities for structural DNA nanotechnology. *Nature Nanotechnology*. 6(12), 763-772.

105. Linko, V., Ora, A., Kostiainen. M.A. (2015). DNA Nanostructures as Smart Drug-Delivery Vehicles and Molecular Devices. *Trends in Biotechnology.* 33(10), 586-594.

106. Wu, N., Zhao, Y. (2020). DNA Nanostructures as Drug Carriers for Cellular Delivery. *Chemical Research in Chinese Universities.* 36(2), 177-184.

107. Obuobi, S., Julin, K., Fredheim, E.G.A., Johannessen, M., Škalko-Basnet, N. (2020). Liposomal delivery of antibiotic loaded nucleic acid nanogels with enhanced drug loading and synergistic anti-inflammatory activity against S. aureus intracellular infections. *Journal of Controlled Release.* 324, 620-632.

108. Wells, C.M., Harris, M., Choi, L., Murali, V.P., Guerra, F.D., Jennings, J.A. (2019). Stimuli-Responsive Drug Release from Smart Polymers. *Journal of Functional Biomaterials.* 10(3), 1-20.

109. Zhao, T., Chen, L., Li, Q., Li, X. (2018). Near-infrared light triggered drug release from mesoporous silica nanoparticles. *Journal of Materials Chemistry B*. 6(44), 7112-7121.

110. Ghosh, S., Qi, R., Carter, K.A., Zhang, G., Pfeifer, B.A., Lovell, J.F. (2019). Loading and Releasing Ciprofloxacin in Photoactivatable Liposomes. *Biochemical Engineering Journal.* 141, 43-48.

111. Geilich, B.M., Gelfat, I., Sridhar, S., van de Ven, A.L., Webster, T.J. (2017). Superparamagnetic iron oxide-encapsulating polymersome nanocarriers for biofilm eradication. *Biomaterials.* 119, 78-85.

112. Li, J., Nickel, R., Wu, J., Lin, F., van Lierop, J., Liu, S. (2019). A new tool to attack biofilms: driving magnetic iron-oxide nanoparticles to disrupt the matrix. *Nanoscale.* 11(14), 6905-6915.

113. Horsley, H., Owen, J., Browning, R., Carugo, D., Malone-Lee, J., Stride, E., *et al.* (2019). Ultrasound-activated microbubbles as a novel intracellular drug delivery system for urinary tract infection. *Journal of Controlled Release.* 301, 166-175.

114. Das, S.S., Bharadwaj, P., Bilal, M., Barani, M., Rahdar, A., Taboada, P., *et al.* (2020). Stimuli-Responsive Polymeric Nanocarriers for Drug Delivery, Imaging, and Theragnosis. *Polymers.* 12(6), 1-45.

115. Pornpattananangkul, D., Olson, S., Aryal, S., Sartor, M., Huang, C-M., Vecchio, K., *et al.* (2010). Stimuli-Responsive Liposome Fusion Mediated by Gold Nanoparticles. *ACS Nano.* 4(4), 1935-1942.

116. Pornpattananangkul, D., Zhang, L., Olson, S., Aryal, S., Obonyo, M., Vecchio, K., *et al.* (2011). Bacterial Toxin-Triggered Drug Release from Gold Nanoparticle-Stabilized Liposomes for the Treatment of Bacterial Infection. *Journal of the American Chemical Society.* 133(11), 4132-4139.

117. Lu, M-M., Ge, Y., Qiu, J., Shao, D., Zhang, Y., Bai, J., *et al.* (2018). Redox/pH dual-controlled release of chlorhexidine and silver ions from biodegradable mesoporous silica nanoparticles against oral biofilms. *International Journal of Nanomedicine.* 13, 7697-7709.

118. Tian, S., Su, L., Liu, Y., Cao, J., Yang, G., Ren, Y., *et al.* (2020). Self-targeting, zwitterionic micellar dispersants enhance antibiotic killing of infectious biofilms-An intravital imaging study in mice. *Science Advances.* 6(33), 1-13.

119. Obuobi, S., Tay, H.K-L., Tram, N.D.T., Selvarajan, V., Khara, J.S., Wang, Y., *et al.* (2019). Facile and efficient encapsulation of antimicrobial peptides via crosslinked DNA nanostructures and their application in wound therapy. *Journal of Controlled Release.* 313, 120-130.

120. Kaszuba, M., Corbett, J., Watson, F.M., Jones, A. (2010). High-concentration zeta potential measurements using light-scattering techniques. *Philosophical Transactions of the Royal Society A: Mathematical, Physical and Engineering Sciences.* 368(1927), 4439-4451.

121. Clogston, J.D., Patri, A.K. (2011). Zeta Potential Measurement. Characterization of Nanoparticles Intended for Drug Delivery. Humana Press. 63-70.

122. Franco, M.S., Gomes, E.R., Roque, M.C., Oliveira, M.C. (2021). Triggered Drug Release From Liposomes: Exploiting the Outer and Inner Tumor Environment. *Frontiers in Oncology*. 11(470), 1-23.

123. Carvalho, P.M., Felício, M.R., Santos, N.C., Gonçalves, S., Domingues, M.M. (2018). Application of Light Scattering Techniques to Nanoparticle Characterization and Development. *Frontiers in Chemistry*. 6, 1-17.

124. McNeil, S.E. (2011). Unique Benefits of Nanotechnology to Drug Delivery and Diagnostics. Characterization of Nanoparticles Intended for Drug Delivery. Humana Press. 3-8.

125. Comission, E. (2011). Comission recommendations of 18 October 2011 on the definition of nanomaterial (2011/696/EU). 38-40. Retrieved from: https://eur-lex.europa.eu/LexUriServ/LexUriServ.do?uri=OJ:L:2011:275:0038:0040:en:PDF (Accessed April 24, 2021).

126. Hoshyar, N., Gray, S., Han, H., Bao, G. (2016). The effect of nanoparticle size on in vivo pharmacokinetics and cellular interaction. *Nanomedicine*. 11(6), 673-692.

127. Škalko, N., Čajkovac, M., Jalšenjak, I. (1992). Liposomes with clindamycin hydrochloride in the therapy of acne vulgaris. *International Journal of Pharmaceutics.* 85(1), 97-101.

128. Šentjurc, M., Vrhovnik, K., Kristl, J. (1999). Liposomes as a topical delivery system: the role of size on transport studied by the EPR imaging method. *Journal of Controlled Release.* 59(1), 87-97.

129. du Plessis, J., Ramachandran, C., Weiner, N., Müller, D.G. (1994). The influence of particle size of liposomes on the deposition of drug into skin. *International Journal of Pharmaceutics. 103*(3), 277-282.

130. Martin, C., Low, W.L., Gupta, A., Amin, M.C., Radecka, I., Britland, S.T., *et al.* (2015). Strategies for antimicrobial drug delivery to biofilm. *Current Pharmaceutical Design.* 21(1), 43-66.

131. Meers, P., Neville, M., Malinin, V., Scotto, A.W., Sardaryan, G., Kurumunda, R., *et al.* (2008). Biofilm penetration, triggered release and in vivo activity of inhaled liposomal amikacin in chronic Pseudomonas aeruginosa lung infections. *Journal of Antimicrobial Chemotherapy.* 61(4):859-868.

132. Danaei, M., Dehghankhold, M., Ataei, S., Hasanzadeh Davarani, F., Javanmard, R., Dokhani, A., *et al.* (2018). Impact of Particle Size and Polydispersity Index on the Clinical Applications of Lipidic Nanocarrier Systems. *Pharmaceutics.* 10(2), 1-17.

133. Sudimack, J.J., Guo, W., Tjarks, W., Lee, R.J. (2002). A novel pH-sensitive liposome formulation containing oleyl alcohol. *Biochimica et Biophysica Acta (BBA) - Biomembranes.* 1564(1), 31-37.

134. Grit, M., Crommelin, D.J.A. (1993). Chemical stability of liposomes: implications for their physical stability. *Chemistry and Physics of Lipids.* 64(1), 3-18.

135. Blanco, E., Shen, H., Ferrari, M. (2015). Principles of nanoparticle design for overcoming biological barriers to drug delivery. *Nature Biotechnology.* 33(9), 941-951.

136. Gratton, S.E.A., Ropp, P.A., Pohlhaus, P.D., Luft, J.C., Madden, V.J., Napier, M.E., *et al.* (2008). The effect of particle design on cellular internalization pathways. *Proceedings of the National Academy of Sciences of the United States of America.* 105(33), 11613-11618.

137. Slomberg, D.L., Lu, Y., Broadnax, A.D., Hunter, R.A., Carpenter, A.W., Schoenfisch, M.H. (2013). Role of Size and Shape on Biofilm Eradication for Nitric Oxide-Releasing Silica Nanoparticles. *ACS Applied Materials and Interfaces.* 5(19), 9322-9329.

138. Zeb, A., Arif, S.T., Malik, M., Shah, F.A., Din, F.U., Qureshi, O.S., *et al.* (2019). Potential of nanoparticulate carriers for improved drug delivery via skin. *Journal of Pharmaceutical Investigation.* 49(5), 485-517.

139. Tak, Y.K., Pal, S., Naoghare, P.K., Rangasamy, S., Song, J.M. (2015). Shape-Dependent Skin Penetration of Silver Nanoparticles: Does It Really Matter? *Scientific Reports.* 5, 1-11.

140. Adams, P.G., Lamoureux, L., Swingle, K.L., Mukundan, H., Montaño, G.A. (2014). Lipopolysaccharide-induced dynamic lipid membrane reorganization: tubules, perforations, and stacks. *Biophysical Journal.* 106(11), 2395-2407.

141. Alam, J.M., Yamazaki, M. (2011). Spontaneous insertion of lipopolysaccharide into lipid membranes from aqueous solution. *Chemistry and Physics of Lipids.* 164(2), 166-174.

142. Jaeger, K-E., Ransac, S., Dijkstra, B.W., Colson, C., van Heuvel, M., Misset, O. (1994). Bacterial lipases. *FEMS Microbiology Reviews.* 15(1), 29-63.

143. Yang, S., Han, X., Yang, Y., Qiao, H., Yu, Z., Liu, Y., *et al.* (2018). Bacteria-Targeting Nanoparticles with Microenvironment-Responsive Antibiotic Release To Eliminate

Intracellular Staphylococcus aureus and Associated Infection. *ACS Applied Materials and Interfaces.* 10(17), 14299-14311.

144. Xiong, M-H., Bao, Y., Yang, X-Z., Wang, Y-C., Sun, B., Wang, J. (2012). Lipase-Sensitive Polymeric Triple-Layered Nanogel for "On-Demand" Drug Delivery. *Journal of the American Chemical Society.* 134(9), 4355-4362.

145. Sugawara, T., Yamashita, D., Kato, K., Peng, Z., Ueda, J., Kaneko, J., *et al.* (2015). Structural basis for pore-forming mechanism of staphylococcal α-hemolysin. *Toxicon.* 108, 226-231.

146. Valeva, A., Hellmann, N., Walev, I., Strand, D., Plate, M., Boukhallouk, F., *et al.* (2006). Evidence That Clustered Phosphocholine Head Groups Serve as Sites for Binding and Assembly of an Oligomeric Protein Pore. *Journal of Biological Chemistry.* 281(36), 26014-26021.

147. Schwiering, M., Brack, A., Stork, R., Hellmann, N. (2013). Lipid and phase specificity of α-toxin from S. aureus. *Biochimica et Biophysica Acta (BBA) - Biomembranes.* 1828(8), 1962-1972.

148. Sanjay, S.T., Zhou, W., Dou, M., Tavakoli, H., Ma, L., Xu, F., *et al.* (2018). Recent advances of controlled drug delivery using microfluidic platforms. *Advanced Drug Delivery Reviews.* 128, 3-28.

149. Biondi, S., Chugunova, E., Panunzio, M. (2016). Studies in Natural Products Chemistry. Chapter 8 - From Natural Products to Drugs: Glyco- and Lipoglycopeptides, a New Generation of Potent Cell Wall Biosynthesis Inhibitors. Elsevier. 50, 249-297.

150. Wilczewska, A.Z., Niemirowicz, K., Markiewicz, K.H., Car, H. (2012). Nanoparticles as drug delivery systems. *Pharmacological Reports.* 64(5), 1020-1037.

151. Srivastava, G.K., Alonso-Alonso, M.L., Fernandez-Bueno, I., Garcia-Gutierrez, M.T., Rull, F., Medina, J., *et al.* (2018). Comparison between direct contact and extract exposure methods for PFO cytotoxicity evaluation. *Scientific Reports.* 8(1), 1-9.

152. Shao, X-R., Wei, X-Q., Song, X., Hao, L-Y., Cai, X-X., Zhang, Z-R., *et al.* (2015). Independent effect of polymeric nanoparticle zeta potential/surface charge, on their cytotoxicity and affinity to cells. *Cell Proliferation.* 48(4), 465-474.

153. Ternullo, S., Basnet, P., Holsæter, A.M., Flaten, G.E., de Weerd, L., Škalko-Basnet, N. (2018). Deformable liposomes for skin therapy with human epidermal growth factor: The effect of liposomal surface charge. *European Journal of Pharmaceutical Sciences.* 125, 163-171.

APPENDICES

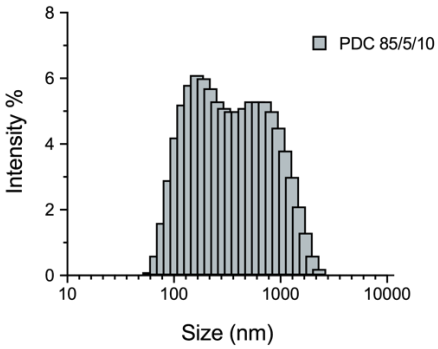

Appendix Figure 1: *Size distribution of PDC 85/5/10 formulation.*

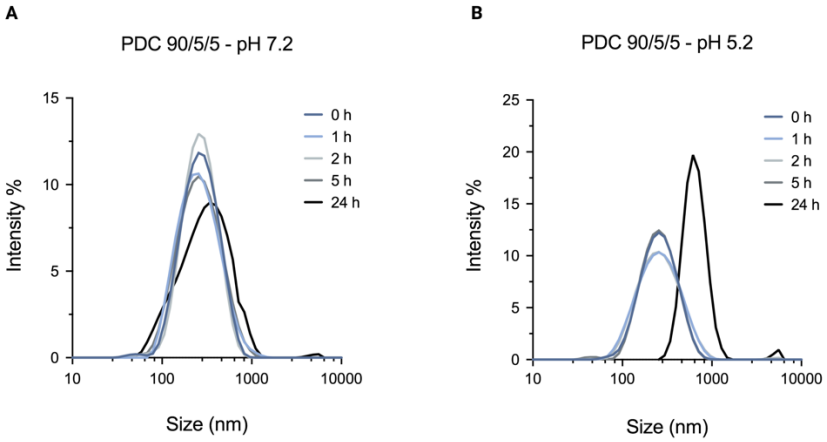

Appendix Figure 2: *pH effect on size distribution of PDC 90/5/5 at A) pH 7.2 and B) pH 5.2.*

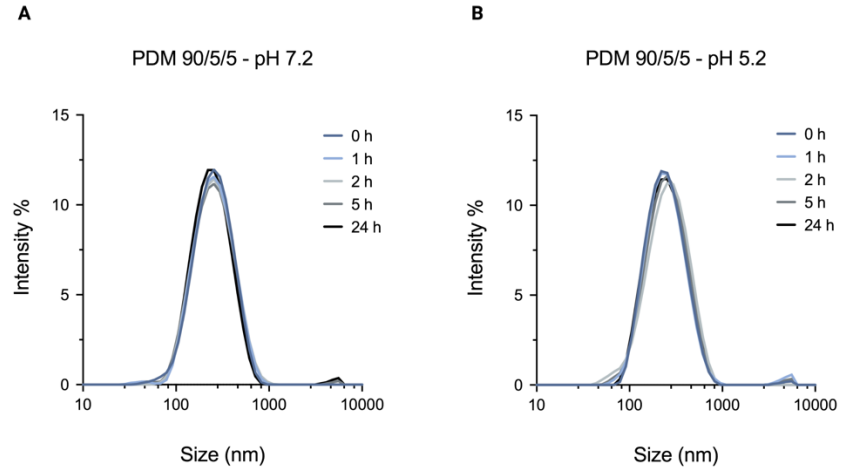

Appendix Figure 3*: pH effect on size distribution of PDM 90/5/5 at A) pH 7.2 and B) pH 5.2.*

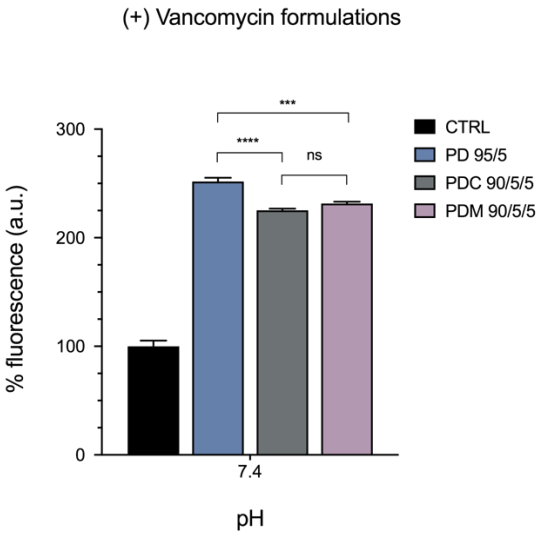

Appendix Figure 4: *Binding affinity to LPS of formulations with vancomycin at physiological pH (7.4).*